Department of Civil and Architectural Engineering
Division of Building Technology

SOUND PROPAGATION AROUND OFF-SHORE WIND TURBINES

Long-Range Parabolic Equation Calculations for Baltic Sea Conditions

Licentiate Thesis

Lisa Johansson

Stockholm 2003

ISRN-KTH-BYT-/R-03/192-SE

ISSN 1651-5536

Postal address
KTH
Dept. of Civil and Architectural Eng.
Div. of Building Technology
SE - 100 44 Stockholm
SWEDEN

Visiting adress
Brinellvägen 34
Stockholm

Phone
Int +46 8 790 8665

Fax
Int +46 8-411 84 32

E-mail
lisa.johansson@byv.kth.se

Preface

This thesis is the result of the project “Ljudspridning kring havsbaserade vindkraftverk” (Sound propagation around off-shore wind turbines); a part of the research program VindForsk. The project was founded by the Swedish Energy Agency, which is gratefully acknowledged. The work was carried out at the Department of Civil and Architectural Engineering, Kungliga Tekniska Högskolan, Stockholm.

I would like to thank my supervisor Professor Sten Ljunggren for giving me the opportunity to carry out this project and for his guidance and support.

I also wish to thank Lars Bergdahl at Chalmers for patiently answering all my questions about water waves; and Ilkka Karasalo and Hans Bodén at the Marcus Wallenberg Laboratory at KTH for helping me with the formulation and programming of the calculation method.

Finally I would also like to thank my colleagues at the Department of Civil and Architectural Engineering, especially Ulrica Kernen and Dr. Olivier Fégeant, for their ideas and support.

Abstract

Low-frequency, long-range sound propagation over a sea surface has been calculated using a wide-angel Cranck-Nicholson Parabolic Equation method. The model is developed to investigate noise from off-shore wind turbines. The calculations are made using normal meteorological conditions of the Baltic Sea. Special consideration has been made to a wind phenomenon called low level jet with strong winds on rather low altitude.

The effects of water waves on sound propagation have been incorporated in the ground boundary condition using a boss model. This way of including roughness in sound propagation models is valid for water wave heights that are small compared to the wave length of the sound. Nevertheless, since only low frequency sound is considered, waves up to the mean wave height of the Baltic Sea can be included in this manner.

The calculation model has been tested against benchmark cases and agrees well with measurements. The calculations show that channelling of sound occurs at downwind conditions and that the sound propagation tends towards cylindrical spreading. The effects of the water waves are found to be fairly small.

Keywords: wind turbine noise, off-shore wind power, long-range sound propagation, parabolic equation, scattering, water waves

Introduction

Wind power is a growing industry. In the year 2001 wind power plants in Sweden produced 0.47 TWh which was an increase of over 30% since 2000. In the Swedish government's energy bill for 2002, it was proposed that the energy production from wind power should increase to 10 TWh by the year 2015. To reach this goal, large off-shore wind power plants must be built. However, the issue of noise from off-shore wind power is not yet fully investigated. According to a literature inventory made by Ljunggren (1999) only a handful measurements of sound propagation over a sea surface have been made. In figure 1 some measurements are compared to different theories.

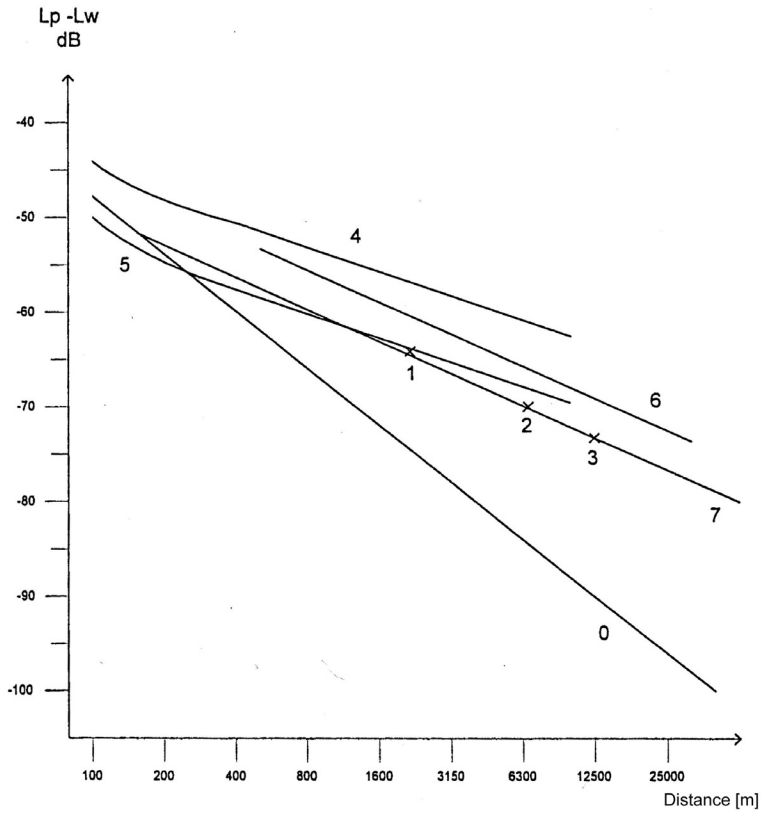

Figure 1 Comparison between measurements and theories regarding long-range sound propagation over a sea surface. The graph shows the difference between sound power level of the source (L_w) and sound pressure level at varying distances (L_p). Line 0 is semi-spherical spreading (- 6 dB/distance doubling). Points 1-3 are measurements. Lines 4-6 represent different calculation methods. Line 7 is cylindrical spreading (- 3 dB/distance doubling) adjusted in height to fit with the measurements (Ljunggren, 1999).

Measurements of low-frequency noise from wind turbines in deserts are presented in Hubbard and Shepherd (1991) and Spera (1994). Deserts have comparable meteorological conditions with those of an ocean. The sand surface has high impedance (at least for low frequencies) and the sand dunes create a smooth roughness on the surface. These measurements show cylindrical propagation (-3 dB per distance doubling) in downwind conditions at long ranges from the wind turbines.

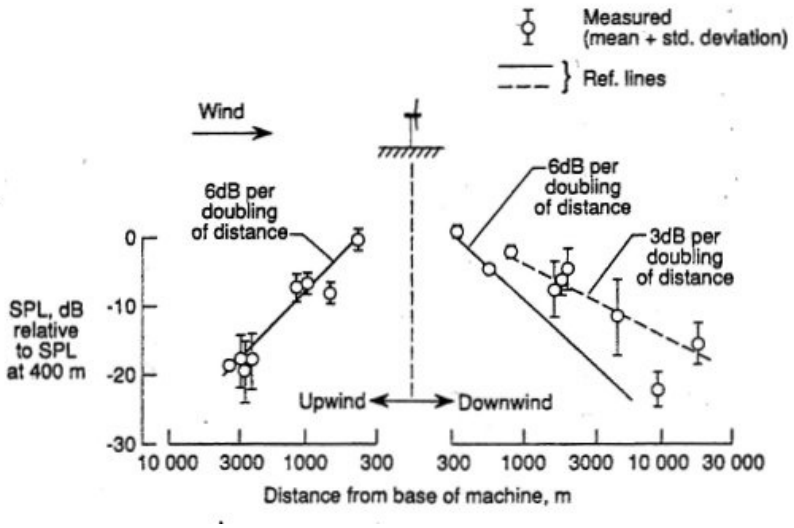

Figure 2 Low-frequency sound measurements from wind turbines presented in Hubbard and Shepherd (1991).

The data collected by Ljunggren (1999) and the measurements presented in Hubbard and Shepherd (1991) and Spera (1994) suggest two important features for long-range sound propagation over a sea surface.

- In downwind conditions, the propagation becomes cylindrical at a certain distance from the source, leading to a sound level reduction of only 3 dB / distance doubling.
- The roughness of the water surface (i.e. the water waves) has little influence on sound propagation.

To investigate these hypotheses, the mechanisms for long-range sound propagation over a sea surface, and state of the art sound propagation models are examined. Scattering models are studied as well as the meteorology and wave climate of the Baltic Sea.

Part I of this thesis contains the background investigations. A thorough literature inventory has been made regarding long-range sound propagation, propagation models, scattering, meteorology, and water wave theory.

In Part II, the calculation model used within the project (a wide-angle CNPE) is described and results from the calculations are presented. Several different scenarios have been investigated with varying surface properties and varying sound speed profiles. Range dependence has also been included to examine what happens when the sound reaches the shore and travels from ocean to inland conditions.

Contents

Part I

1. Atmospheric sound propagation

Sound waves are always affected by the properties of their propagation medium. This chapter will describe atmospheric effects on sound propagation. The three most important features of atmospheric sound propagation are absorption, refraction and turbulence. A thorough description of this topic can be found in the paper by Embleton (1996).

1.1. Absorption

A sound wave propagating through the atmosphere, or through any other fluid, will interact with the molecules of the fluid. The wave will make the molecules rotate and vibrate, thereby transferring energy from the sound wave to the air. The viscosity of the air will also consume energy from the sound wave. The combined effect of these two features is called absorption. The absorption depends on the temperature, the relative humidity and the pressure of the air. The absorption increases rapidly with the frequency of the sound, with the result that the low frequencies of a sound source is of much more importance than the high frequencies for long range sound propagation.

The international standard ISO 9613-1 describes how to calculate the absorption coefficient, defined as the sound level attenuation due to absorption per kilometre. The standard also includes tables for common atmospheric conditions. For typical Swedish conditions, Larsson (1997) has calculated absorption coefficients based on 30 years of meteorological data. These are suitable to use when calculating sound propagation in Sweden since the standardized global value overestimates the absorption at high frequencies for Swedish conditions.

Frequency [Hz]	*63*	*125*	*250*	*500*	*1000*	*2000*	*4000*	*8000*
Luleå	0,12	0,4	0,9	2,1	5,0	13,8	40,1	111,5
Frösön	0,12	0,4	0,9	1,9	4,6	13,5	41,6	118,8
Uppsala	0,11	0,4	0,9	1,9	4,3	11,9	37,5	114,6
Säve	0,11	0,4	0,9	1,9	4,1	10,9	35,0	111,1
Bredåkra	0,11	0,4	0,9	1,9	4,0	10,9	35,2	111,9
Ljungbyhed	0,11	0,4	0,9	1,9	4,0	10,8	34,7	111,4
Global		0,4	1,1	2,4	5,9	18,8	53,9	129,3

Table 1. Mean absorption per frequency is given as the decrease in decibels per kilometre, dB/km. Swedish values are calculated by Larsson (1997), the global value is from ISO 9613-1.

1.2. Refraction

Sound waves can be represented as rays travelling through the atmosphere. The path that the rays follow is determined by how the sound speed varies in the atmosphere. The sound speed is a function of the wind speed, the wind direction and the temperature; hence, variations in these properties will cause variations in the sound speed. The bending of sound rays due to varying sound speed is called refraction.

Refraction can be upwards or downwards depending on whether the rays are turning away from or towards the ground surface. Upward refraction is caused by a negative temperature gradient and/or a wind blowing in the direction opposite of the sound propagation. Since the sound rays are turned away from the surface and up into the atmosphere, upward refraction will reduce the sound level near the ground and can also cause shadow zones.

Downward refraction is caused by a positive temperature gradient and/or a wind blowing in the same direction as the sound propagation. In this case, the sound rays are concentrated near the ground. Downward refraction will therefore enhance long-range sound propagation. If the propagation path is long enough, the sound rays will be reflected one or multiple times by the surface, making the properties of the surface very important.

In the case of long range sound propagation in a downwards refracting atmosphere sound waves may be reflected more than once. The paths of the reflected waves are longer than the path of the direct wave. For continuous, time-invariant sound that shows as interference between the waves due to differences in phase. For an impulse noise there will be a sinusoidal pattern in the measured sound.

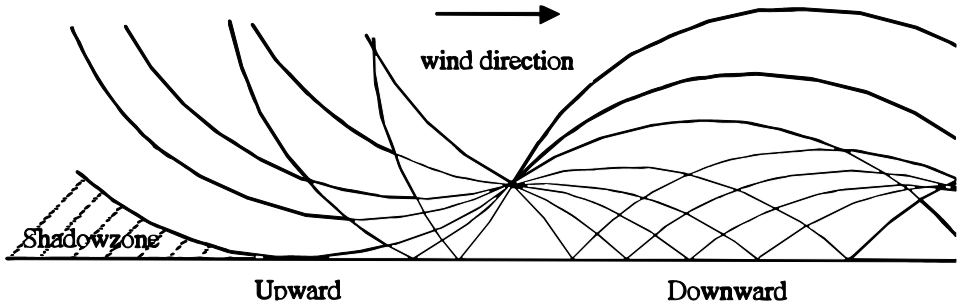

Figure 3. A schematic figure showing sound rays in a refracting atmosphere. Upwind the sound is refracted upwards creating a silent shadow zone. Downwind the sound is refracted downwards and focused near the ground. Downward refraction is therefore enhancing long-range sound propagation.

1.2.1. Refractive index and effective sound speed

The strength of the refraction can be described by the refractive index; n. To calculate the refracting index, the effective sound speed is defined as $c_{eff} = c + u$, where u is the wind speed in the direction of sound propagation and c is the sound speed in the atmosphere. The sound speed c is related to the temperature as $c = c_0\sqrt{T/T_0}$ where c_0 is 331 m/s, T is the current temperature and T_0 is 273 K. The refractive index is then $n = c_0/c_{eff}$.

Using the effective sound speed is an easy way to include medium motion and refraction effects in sound propagation models. However, it can lead to errors. According to Ostashev (1997, p. 86), especially ray tracing are methods sensitive to it, since it leads to errors in the phase shifts. Nevertheless, keeping this in mind, the effective sound speed approximation is valid as long as the elevation angle to the ground is relatively small; $|z - z_s| << \sqrt{x^2 - y^2}$ (Salomons, 2001, p. 146).

1.3. Effects of turbulence

Turbulence can be regarded as random variations of the properties of the air. Since the sound speed is determined by these atmospheric properties; the sound speed will also vary correspondingly due to turbulence. The sound field will be diffracted by the turbulence eddies and will therefore become more diffuse than in a homogenous atmosphere. Turbulence can also scatter sound into shadow zones. Depending on the size of the turbulence eddies it will affect the sound in different ways. Large-scale turbulence mainly causes variations in phase, while turbulence of smaller scale causes variations in amplitude (Wilson et al., 1999). In weak turbulence theory the incoming sound wave is assumed to be undisturbed when it reaches the turbulence eddies. For such a case, the eddies distorts the sound amplitude and phase rather effectively. However, for strong turbulence or long range sound propagation, the incoming wave cannot be assumed to be undisturbed. Since it already has been randomly distorted the effect of turbulence seems to be saturated and further turbulence will not have much impact on the average sound amplitude (Daigle et al. 1983).

To include turbulence in sound propagation models it must first be properly described. Since it is a random phenomenon, the usual method is to describe it using statistics. Ostashev (1997, ch. 6) does this by calculating the structure function of the random fields (i.e. the temperature; $\tilde{T}$, the molecular concentration of some component of the air; $\tilde{C}$ and the wind; u_i (i = 1, 2, 3)). Ostashev also expresses the cross-correlation function between $\tilde{T}$ and $\tilde{C}$ (the wind is assumed to be uncorrelated with the temperature and the concentrations) and their three-dimensional spectral densities (Φ_T, Φ_C, Φ_{ij} and Φ_{CT}).

There are three commonly used turbulence spectra that simplify the calculation of these statistical properties, the Kolmogorov, the Gaussian and the von Kármán spectrum. Expressions for these spectra can be found in Ostashev (1997, ch. 6) and Salomons (2001, ch. I.7).

These turbulence spectra describe turbulence of all scales and are not especially developed with sound propagation in mind. According to Wilson et al. (1999) it is unnecessary to try to model all parts of the turbulence accurately since only some of it affect sound propagation. Wilson et al. divide the turbulence length scale into three subranges, the energy-containing subrange, the inertial subrange and the dissipation subrange. Of these three, only the energy-containing subrange and the inertial subrange will affect sound propagation. The motions in the dissipation subrange are too small compared to most acoustic wavelengths to have any impact. Wilson et al. (1999) suggest that an acoustical filter should be chosen based on the actual propagation geometry and investigated frequencies. Then, the turbulence spectrum that best describes the turbulence within this acoustical filter should be chosen. Wilson (2000) has also developed a three-dimensional spectrum, based on the von Kármán spectrum, and suited for sound propagation calculations.

2. Meteorology

Knowledge in meteorology is helpful when doing sound propagation calculations. Therefore, this chapter will describe some useful parts of boundary layer meteorology. The two by far most important properties of the atmosphere are the wind velocity profile and the temperature profile. Beside that, the density and the humidity of the air are needed for calculating absorption and the molar concentration of the different components of the air could be used when calculating turbulence. Absorption and turbulence have already been covered and are not included in the calculation model developed within this project so this chapter will only focus on wind velocity and temperature.

2.1. Temperature

When a small volume of air moves upwards in the atmosphere it will expand since the atmospheric pressure is decreasing with height. The work needed to perform this expansion is taken from the volume itself and hence, the temperature of the volume is decreased. The atmospheric pressure decreases linearly with height and the temperature of a small volume travelling upwards will therefore also decrease linearly with height. This decrease is 1°C/100 m.

If also the temperature in the atmosphere surrounding the small volume of air is decreasing with 1°C/100 m there will always be temperature equilibrium between the small volume and the atmosphere. This kind of atmosphere is said to be neutrally stratified. On the other hand, if the temperature in the atmosphere is decreasing with more than 1°C/100 m, the small volume travelling upwards will be warmer and have lower density than the surrounding air. It will therefore be forced to move upwards even more. This kind of atmosphere enhances vertical movements and is said to have unstable stratification. Convective clouds like thunder clouds can be formed in an unstable atmosphere.

If the temperature is decreasing with less than 1°C/100 m, the small volume will be colder and heavier than the surrounding air. It will be forced back towards its original height. This kind of atmosphere prevents vertical movements and is said to have stable stratification.

Normally (at least at daytime) the temperature in the atmosphere is decreasing with height but sometimes there can be an inversion, a layer where the temperature is increasing instead. Such a layer is very stable and it prevents vertical movements in the atmosphere effectively. Inversions are common during cold winter days and are often visible as they work like lids keeping smoke or fog near the ground.

2.2. Wind velocity

The part of the atmosphere that is of interest for normal sound propagation is the so-called friction layer, which is the lowest kilometre of the troposphere. In this layer, the wind is affected by friction from the ground surface. The friction layer is divided into two sub-layers; the surface layer and the Ekman layer.

The thickness of the surface layer varies between just a few metres to about 100 metre above the ground, most often being around 10 – 20 metres. In the surface layer the wind speed profile usually follows the so-called logarithmic wind law:

$$u(z) = \frac{u*}{\kappa} \ln\left(\frac{z}{z_0}\right) \qquad (1)$$

where u is the wind speed, u* is the friction speed which is a measure of the turbulent friction (a higher value of u* means that the sound speed is increasing faster with height), κ is the von Kármán constant which is dimensionless and has the value 0.4, z is the height and z_0 is the roughness parameter of the surface. The roughness parameter is about one tenth of the roughness elements on the surface. For a shortly trimmed lawn; $z_0 \approx 1$ mm, and for a forest; $z_0 \approx 1$ m. Of course, undulations of the surface itself also affect the roughness parameter. A water surface has a very low roughness parameter, even when there are waves (Lange and Højstrup, 1999).

The Ekman layer is named after the Swedish oceanographer V. W. Ekman. He found that the direction of the ocean currents turns like a spiral with depth, and the same thing happens in the atmosphere. This phenomenon can be explained by studying the force balance in the atmosphere. Above the friction layer the forces affecting a small volume of air are only the gradient force, created by variations in atmospheric pressure, and the coriolis force, which is caused by the rotation of the earth. In the surface layer there is also a frictional force. The force balances are shown in figure 4.

In figure 4 the isobars (lines with constant pressure) are assumed to be parallel. Above the friction layer, the wind is blowing parallel to the isobars. This wind is called the gradient wind and it is created by differences in atmospheric pressure. Further down in the atmosphere the frictional force causes the wind to turn. Since the frictional force increases closer to the ground the wind will turn even more, thus creating the spiral shape of the wind direction profile that is characteristic for the Ekman layer.

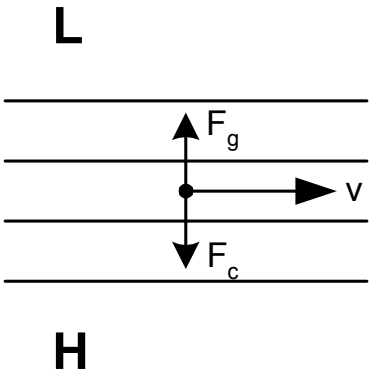

Figure 4a. Force balance above the friction layer. L and H represents low and high atmospheric pressure. The gradient wind is blowing parallel to the isobars. The gradient force (F_g) is equal to the coriolis force (F_c) which is always perpendicular to the wind direction (V) and pointing to the right.

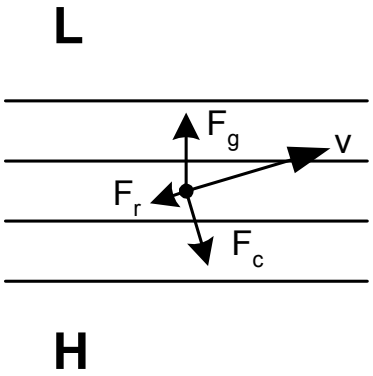

Figure 4b. Force balance in the friction layer. The gradient force is the same as in fig 4a but there is also a frictional force (F_r) pointing in the opposite direction of the wind. To obtain a balance between the forces the wind must cross the isobars. The coriolis force is still perpendicular and to the right of the wind direction.

2.2.1. Low-level jets

Low level jets are strong winds blowing at a relatively low altitude. They can be caused by several factors and are observed over large flat areas, such as oceans, seas and deserts. In measurements over the Baltic Sea made by Källstrand (1998) during spring, low level jets occurred in 38 out of 52 observations. The two most common factors causing these low level jets were inertial oscillations and the sea breeze.

Low level jets due to inertial oscillations are created when warm inland air flows out over a cold water surface. In the atmospheric layers closest to the surface, turbulence dies out and the shear stress between these layers becomes almost zero, thus allowing the wind speed to increase drastically with height. Since the oscillation is driven by the difference in temperature between the air and the water surface, this type of low level jet is most common during spring.

It takes some time for the atmosphere to fully develop a low level jet like this. In that time, the layers of warm air will travel over the water surface. After about 5 – 7 hours the wind speed in the low level jet will have reached its maximum. With an initial wind speed of 10 m/s the air can travel from one side of the Baltic Sea to the other in that time. A wind blowing from the Baltic States will therefore be at its maximum velocity when in reaches Gotland. The oscillation normally lasts about 14 hours (Källstrand 1998). Wind speed and direction profiles of a low level jet caused by inertial oscillation are given in figure 5.

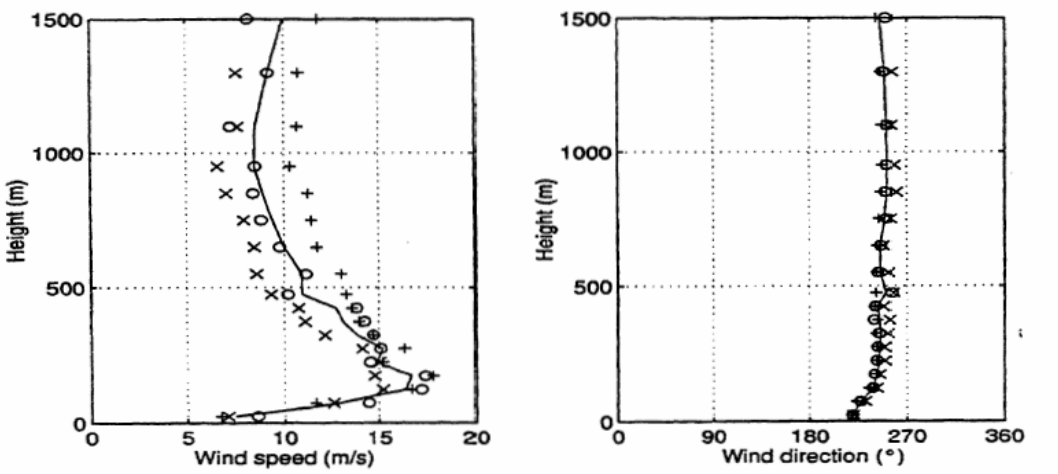

Figure 5. Typical wind speed and direction profiles for a low level jet caused by inertial oscillation (Källstrand 1998).

Another cause of low level jets is the sea breeze. Sea breeze is a very common phenomenon along the coasts of Sweden during spring and summer. It is created by the summer sun that warms the land along the coast. The warm ground will in its turn heat up the air just above it; which will rise. At a certain altitude the warm air will start flowing out over the sea. An empty space is created over land and air from just above the water surface will start blowing in, creating a circulation system along the coast.

Wind speed and wind direction profiles a sea breeze are depicted in figure 6. A typical feature of this kind of low level jet is the significant change in the direction of the wind. The wind is always blowing onshore near ground, while it is reversed higher up due to the circulation process described above. Low level jets caused by inertial oscillation do not exhibit this change in wind direction.

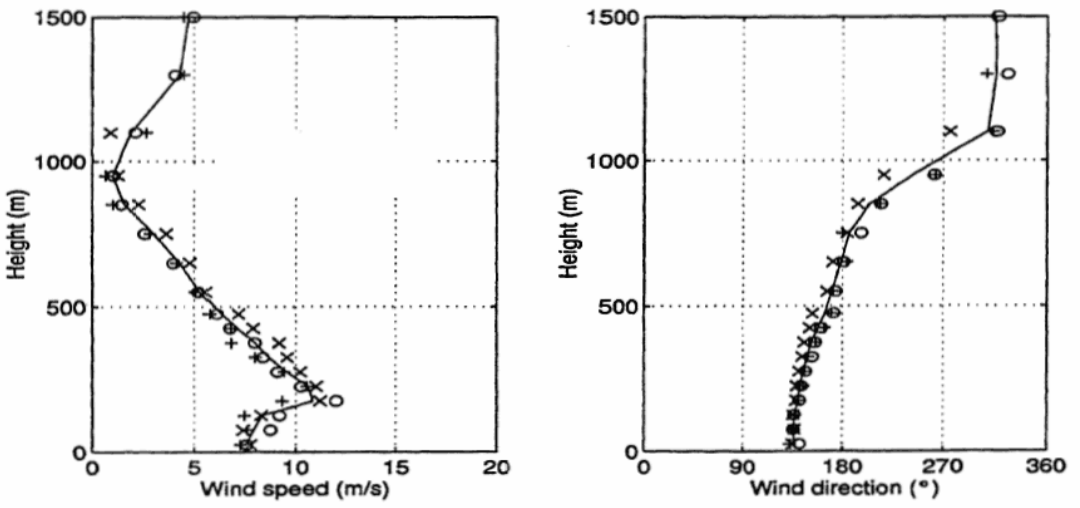

Figure 6. Typical wind speed and direction profiles for a sea breeze (Källstrand 1998).

2.2.2. Winds in the Baltic Sea

SMHI (the Swedish Meteorological and Hydrological Institute) continuously measures the wind speed and direction in several places in the Baltic Sea. According to Mårtensson and Bergdahl (1987) the average wind speed at 10 m height is 8.32 m/s at Ölands Södra Grund and 7.09 m/s at Hoburg (just south of Gotland).

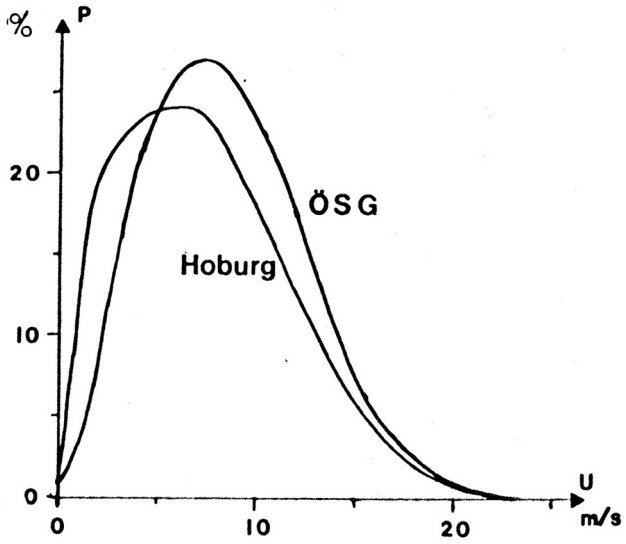

Figure 7 Wind speed probability functions for Ölands Södra Grund (ÖSG) and Hoburg (Mårtensson and Bergdahl, 1987).

2.3. Turbulence

As mentioned earlier, turbulence can be regarded as random variations in the properties of the air, including the wind speed and the wind direction. Turbulence can either be mechanically or thermally created. Mechanical turbulence appears when the wind is blowing over uneven ground and the surface roughness causes small eddies of rotating air. Thermal turbulence is created by the radiation from the sun. The sun warms the ground which in its turn warms the air. If this heating is irregular (due to different properties of the surface for example) or if it is very rapid, the heated air will be surrounded by colder air. Since warm air is lighter than cold air it will travel upwards in eddies.

The turbulence eddies vary a lot in size. Generally the size of the eddies increases with height. The scale of the eddies is an important property which is described by an outer and an inner scale, where the outer scale, L, is the size of the largest eddies and the inner scale, l_0, is the size of the smallest eddies. Salomons (2001, p. 207) find that it is quite possible that l_0 can be of three orders of magnitude smaller than L.

3. Water waves

A flat water surface can be regarded as totally reflecting for sound. It is, however, unrealistic to assume that a sea surface is flat. Since a rough surface has somewhat different reflecting properties than the corresponding flat surface (chapter 4.3); a calculation model for long-range sound propagation over a sea surface should include the effects of water waves. To do this, knowledge of water waves and the wave climate in the region of interest is of importance.

3.1. A general description of water waves

A sea surface has a spectrum of different kinds of water waves with different amplitudes and wavelengths. The largest waves are caused by the rotation of the earth - they can have a period of several months. The smallest waves are the capillary waves, which have a period of about a second and an amplitude of a couple of centimetres. Different wave types and their size are illustrated in figure 8.

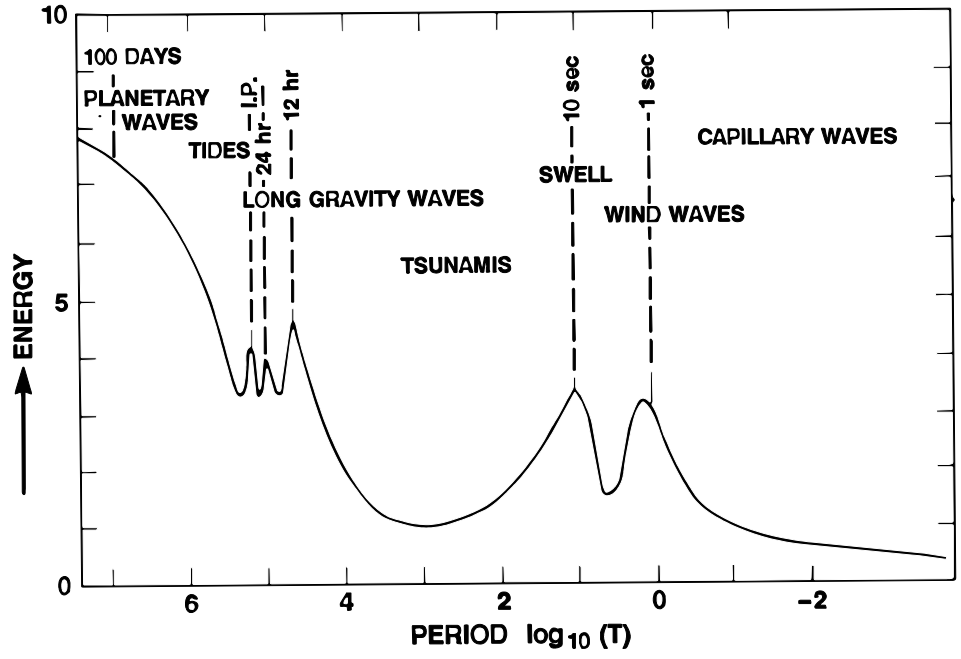

Figure 8. Different wave types and their period (Khandekar 1989).

3.2. Modelling water waves

Due to the complexity of the water waves it is hard, not to say impossible, to exactly describe a water surface explicitly. Instead, water surfaces are most often described by their spectrum or by some other statistical method. The first attempts to describe the sea surface were done for the shipping industry and consisted of simple tables of expected wave heights at certain wind conditions. During the Second World War empirical diagrams were obtained for the relation between water wave frequency, amplitude and wind speed.

Today most wave models are based on the energy balance equation:

$$\frac{\partial}{\partial t} E(f,\theta,\mathbf{x},t) + \mathbf{c}_g \bullet \nabla E = S(f,\theta,\mathbf{x},t) \qquad (2)$$

where E is the energy density of the wave field, f is the frequency, θ is the propagation angle, c_g is the group speed of the waves (in deep water) and S is a source function. The effect of wind and other atmospheric conditions are included in *S*. Though this energy balance is an exact description of wave propagation, approximate methods must be used to obtain *S* (Khandekar 1989).

3.3. Wind waves

The wave type that is of interest when studying scattering of sound by a sea surface is the wind wave (also called gravity wave). Wind waves are created by the wind, hence their name. The damping forces acting on the waves are gravity and, to some extent, surface tension.

Wind waves can be described by linear theory which is based on a couple of simplifications:

- The water is of constant depth and the depth is large compared to a wavelength
- The wavelength is in its turn large compared to the wave height
- The waves are two-dimensional and of constant form
- The water is incompressible
- Viscosity, surface tension and turbulence are neglected

Linear theory yields sinusoidal waves for which the water surface can be modelled by a spectrum of waves with varying wavelengths and amplitudes (Bergdahl 2002).

The wind waves are not transporting any water, only the wave movement itself is propagating over the water surface. The water particles perform a circular movement when the wave is passing by. If the water depth is limited the circular movement is restricted and becomes elliptical (figure 9).

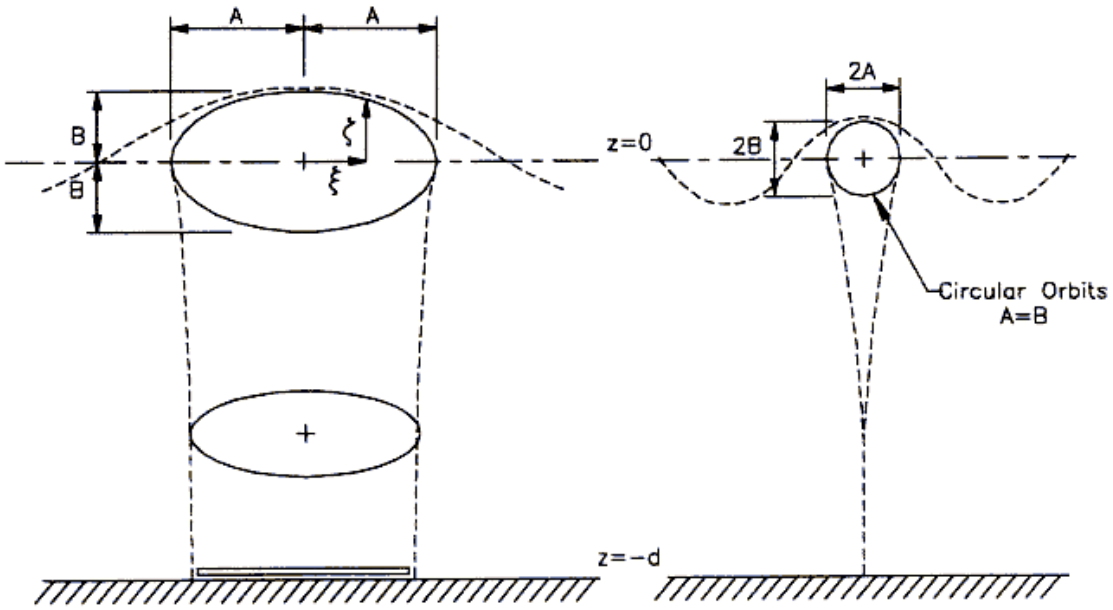

Figure 9. Particle movements for a wave in shallow water (to the left) and deep water (to the right). The particle path is circular in deep waters while it for shallow waters is restricted and therefore elliptical (Bergdahl 2002).

In wave measurements it is often the period that is measured rather than the wavelength. The relation between the period and the wavelength is therefore of importance and it varies with the depth of the water (Bergdahl 2002):

In deep water, d>>L: $$L = \frac{gT^2}{2\pi} \quad (3)$$

In shallow water, d<<L: $$L = T\sqrt{gd} \quad (4)$$

where L is the wavelength, g the constant of gravity, T the period of the wave and d the depth of the water.

As long as the wind that creates the water waves is blowing in the same direction; the waves will grow until a balance is reached between the energy given by the wind and the energy lost due to gravity, inner friction and surface tension. Energy is given to the wave by two processes; from the friction between the wind and the water surface and from the pressure difference between the upwind and downwind side of the wave (Bergdahl 2002).

To begin with, the wind must have a certain speed to be able to create and maintain waves; this speed is about 1.1 m/s (Reinius, p 40, 1963). The waves can travel faster than the wind speed since the particle velocity in the wave is lower than the speed of the wave. Therefore, energy can still be transferred to the wave by friction even if the wind speed is slower than the wave (Reinius, p 40, 1963). Even so, for simplicity the maximum wave speed can be set as the speed of the wind (Bergdahl 2002). As the wave amplitude grows the speed of the wave increases as: $C = 1.25\sqrt{L}$ (valid for deep water).

The size of the waves depends not only on the speed of the wind but also the duration of the wind and the distance in which the wind is blowing in the same direction (the fetch). Over smaller waters, the fetch is often the distance to the opposite shore. Over an ocean or a sea, the wind seldom blows in the same direction and speed from one shore to another so then the fetch is the estimated region with homogenous wind conditions.

Reinius (p 46, 1963) shows in a couple of diagrams of how the wave height and period varies with wind speed and fetch. (The diagrams are originally in Swedish but have been translated for this report.)

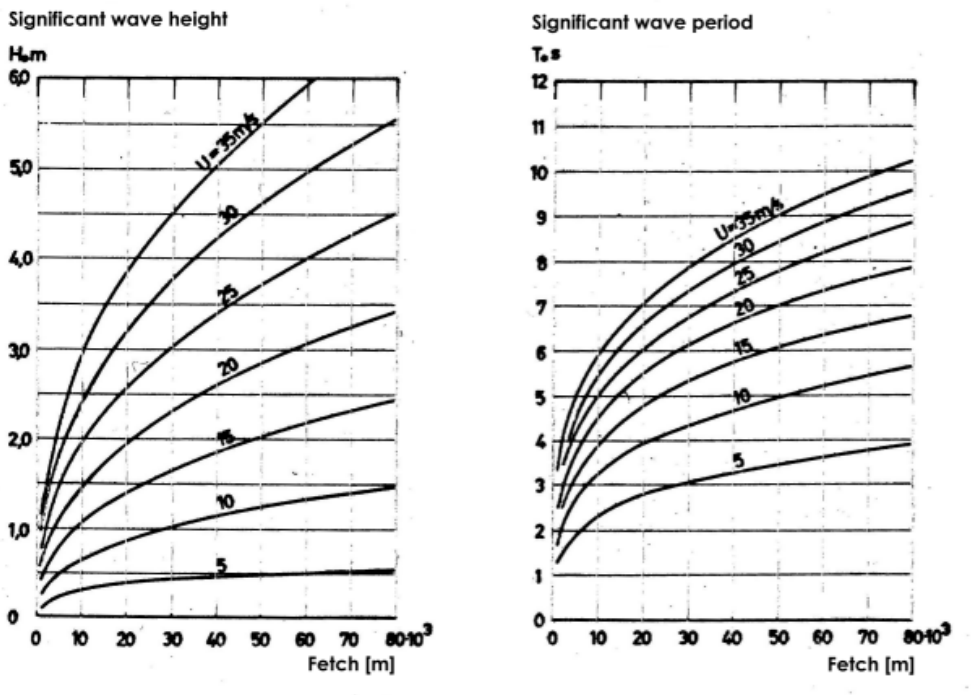

Figure 10. Diagrams showing for different wind speeds (U) the significant wave height as a function of fetch and the significant wave period as a function of fetch (Reinius, p 46, 1963).

3.3.1. Waves in the Baltic Sea

Long-term measurements of the wave climate at Ölands södra grund and Hoburg in the southern Baltic Sea have been presented by Mårtensson and Bergdahl (1987). The measurements were done during 1979 and 1980. They show that the wave climate is "rather mild". The mean wave height at both Ölands Södra Grund and Hoburg is around 1 m and the mean period is around 4 s (Mårtensson and Bergdahl, 1987). (Note that the wave height, H_s, is the height from the bottom of the wave to the top of the wave; which equals 2B in figure 9.)

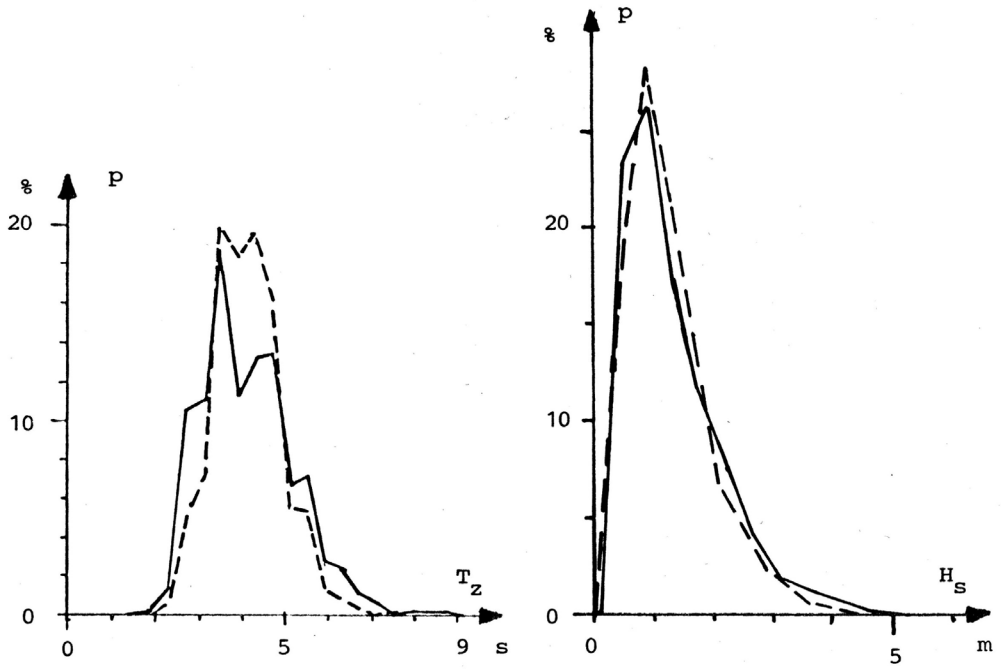

Figure 11 Wave period (T_z) and height (H_s) probability functions for Ölands Södra Grund (solid line) and Hoburg (dashed line) (Mårtensson and Bergdahl, 1987).

4. Surface interaction

When a wave travels in a bounded atmosphere (that is, an atmosphere that is infinite in one direction but is restricted in the other by a surface) four different kinds of waves can appear; an undisturbed direct wave between the source and the receiver, a reflected wave, a ground wave and a surface wave. The three latter waves appear only if the travel path of the sound waves is cut off by a surface and they will be described in this chapter.

4.1. Reflection

Figure 12 describes the geometry of the case of a sound wave travelling from a source to a receiver in the vicinity of a reflecting surface.

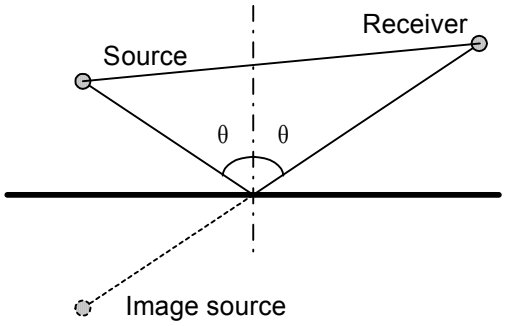

Figure 12 A sound wave reflected at a surface will have equal angles of incidence and reflection, θ ("law of mirrors"). The total field at the receiver will be the sum of the direct field and the reflected field where the reflected field can be seen as a field coming directly from a mirror source.

The reflected sound wave can be regarded as a wave coming from an apparent image source. If the source is located at $(0, 0, z_0)$ and the reflecting surface is at $z = 0$, then the image source will be at $(0, 0, -z_0)$. The law of mirror holds so the reflected angle is always the same as the incident angle.

The amplitude of the image source is the reflection coefficient times the amplitude of the real source. If the surface impedance is finite, the reflection coefficient will be less than one and some sound energy will be lost at the reflection. The formula for the reflection coefficient depends on the wave type. In most cases the formula for plane wave reflection can be used:

$$R \cong \frac{Z\cos\theta - 1}{Z\cos\theta + 1} \tag{5}$$

where R is the reflection coefficient and θ is the angle of incidence. Z is the normalised surface impedance for which $Z = Z_s/(\rho c)_{air}$ and Z_s is the specific surface impedance. Z_s equals the sound pressure divided by the fluid velocity normal to the surface; $Z_s = p/(\mathbf{v}\bullet\mathbf{n})$. Equation (5) is valid as long as the cumulative height of the source and the receiver is more than one wavelength.

It is quite a complex matter to describe a real surface and its impedance and several methods to do this are available. One method of calculating the normalised impedance Z using the effective flow resistivity as only parameter can be found in Embelton et al. (1983):

$$Z = 1 + 9.08\left(\frac{f}{\sigma}\right)^{-0,75} + 11.9i\left(\frac{f}{\sigma}\right)^{-0,73} \tag{6}$$

where f is the frequency and σ the effective flow resistivity of the ground. Equation (6) is originally from Delany and Bazley (1970) but a sign have been changed by Embelton et al. (1983) to make the model accurate for a time-dependence of ($e^{-i\omega t}$). Values of σ for some common ground surfaces are given in table 2.

Surface type	*Flow resistivity [csg rayls]* *(1 csg rayls = 1000 Pa s/m^2)*
Dry, newly fallen snow, 10 cm deep	15 - 30
In forest, pine or hemlock	20-80
Grass covered fields	150 - 300
Sandy, hard-packed silt	800 - 2 500
Exposed, rain-packed earth	4 000 – 8 000
Asphalt sealed by dust	>20 000

Table 2 Effective flow resistivity for different types of natural and artificial surfaces (Embelton et al. 1983).

Three more elaborate models are compared by Raspet and Sprague (1990):

- the so-called rigid back layer which assumes that the surface consists of a rigid layer covered with a porous material.
- a method by Donato where the material's porosity times the wave number is decreasing exponentially with depth.
- a model where the material's porosity is decreasing with depth, developed by Attenborough.

Raspet and Sprague (1990) found that the three different methods gave more or less similar results.

4.2. Ground and surface waves

Ground waves and surface waves can be created if certain conditions regarding the surface impedance are fulfilled. Even though both wave types have been theoretically accepted for some time, they can be difficult to measure. Daigle and Embelton (1990) explain that ground waves are created when a curved wave is incident on a surface and hits the surface at an angle. The wave will strike the surface with different phase at different places. The ground waves propagate in the ground itself. They can only appear in surfaces that have finite impedance. Ground waves are of rather little importance for long range sound propagation.

4.2.1. Surface waves

Surface waves might appear when a sound wave is travelling over a surface with finite impedance. They are mainly a low-frequency phenomenon and they are created by the horizontal movements of the incoming wave and the vertical movements of either a ground wave or of air in the pores of the surface. For rigid surfaces, surface waves can exist if the surface is porous enough. The primary condition for the creation of surface waves is that the reactance of the surface (the imaginary part of the surface impedance) must be larger than the resistance (the real part of the surface impedance). The reactance must also be positive so that the surface acts in a spring-like manner.

According to Stinson and Daigle (1997) most natural ground surfaces have the properties needed for the creation of surface waves. They are, however, most pronounced when the surface consists of a thin porous layer over hard ground, for example a thin layer of newly fallen snow over an otherwise hard surface. The air in the porous layer will act as a spring enhancing the vertical movements of the surface (figure 13). Stinson and Daigle (1997) found that the surface waves are to be expected when the reactance of the surface is larger than the resistance and in the range $2 < \mathrm{Im}(Z)/\rho c < 6$. If these condition holds, energy from the sound wave will be trapped near the surface and create a surface wave that propagates cylindrically and independently of the body wave in the atmosphere.

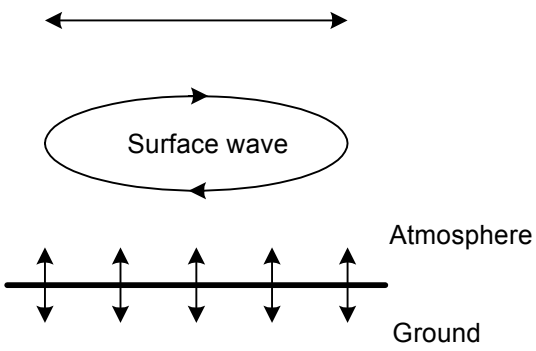

Figure 13 A surface wave, created by vertical oscillations of the ground and horizontal oscillations of the atmosphere.

The surface wave has a phase speed that is less than the speed of sound in the air. It can therefore be visible when measuring acoustic pulses as an echo arriving to the receiver slightly after the direct pulse. Such measurements have been made by Daigle et al. (1996). For continuous sound the surface wave is not explicitly visible but it gives a contribution to the sound level near the ground.

4.3. Rough surfaces

When a sound wave is reflected at a smooth surface, all incoming rays of the wave field will be reflected at the same angle. An incoming plane wave will also be reflected as a plane wave. The phase difference between different parts of the wave will be the same as before the reflection and the reflected sound field will therefore be coherent.

If the surface is rough however, the incoming rays will be reflected at different angles. The travel times before reflection will also vary and there will be varying phase shifts for different rays. Because of this, the reflected rays will interfere with each other and with the incoming rays. The reflected field will have a coherent part, smaller than for smooth surface reflection, and an incoherent, or diffuse, part. As the roughness of the surface increases the diffuse field will become larger than the coherent field (Ogilvy, 1991).

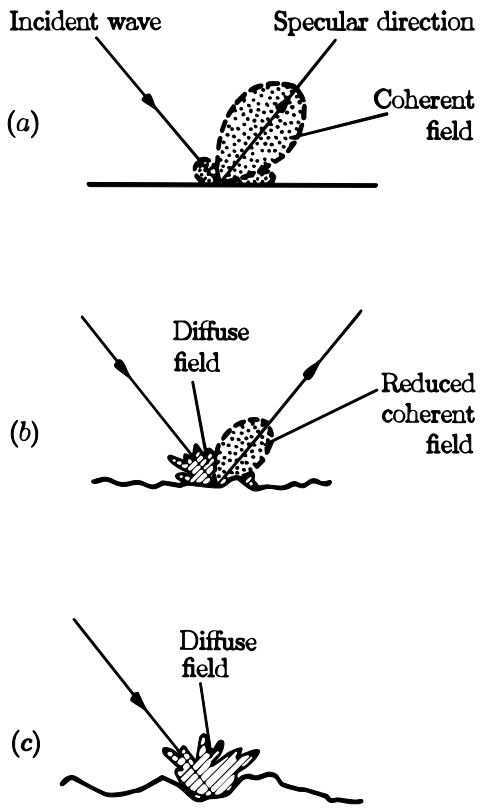

Figure 14 Figure showing how the coherent reflected field is decreasing and the diffuse field is increasing when the roughness of a surface grows larger (Ogilvy, 1991).

Boulanger et al. (1998) explain that at a receiver, all broadband sound that has been reflected by a surface (smooth or rough) will show a sound level minimum at a certain frequency. A soft surface will yield a minimum at a lower frequency than a hard. Surface roughness will also move the sound level minimum towards a lower frequency. Hence, roughness tends to make a surface acoustically softer.

5. Sound propagation models

There are three commonly used methods for calculating sound propagation; the Parabolic Equation method (PE), the Fast Field Program (FFP) and ray tracing. The PE and the FFP are numerical methods while ray tracing is analytical. Nevertheless, except for quite simple cases, numerical methods must still be used to solve the equations in ray theory. A good review and comparison of these models with extensive references can be found in an article by Attenborough et al. (1995).

5.1. The Fast Field Program

Salomons (2001, p. 49) explains the fundamental method of the Fast Field Program: "The Fast Field Program (FFP method) is based on a Fourier transformation of the wave equation from the horizontal spatial domain to the horizontal wave number domain. The transformed wave equation is solved numerically, and the solution is transformed back to the spatial domain by an inverse Fourier transformation."

This transformation from the spatial domain to the wave number domain demands that the atmospheric and ground conditions are independent of range. That means that the atmosphere must be layered and each layer must be constant. It also means that the atmospheric properties and the ground surface cannot change along the propagation path.

One way of doing the transformation is to start with the wave equation for an inhomogeneous atmosphere:

$$\frac{1}{\rho_{av}}\nabla\cdot(\rho_{av}\nabla\phi_v)-\frac{1}{c^2}\frac{D^2\phi_v}{Dt^2}=0 \qquad (7)$$

and

$$p = -\rho_{av} \frac{D\phi_v}{Dt} \tag{8}$$

where ρ_{av} is the average atmospheric density (as a function of height), ϕ_v is the velocity potential, c is the sound speed and p the sound pressure. D/Dt is the total derative for a frame moving with the medium; $D/Dt = \partial/\partial t + \mathbf{v}_{av}\cdot\nabla$ (Salomons 2001, p. 144).

Doing a double Fourier transform of (7) and (8) from the spatial domain (x, y, z) to the horizontal wave number domain (k_x, k_y, z) and neglecting small terms, the homogeneous Helmholtz equation in the wave number domain is derived:

$$k_m^2 \frac{\partial}{\partial z}(k_m^{-2} \frac{\partial P}{\partial z}) + k_{mz}^2 P = 0 \tag{9}$$

where P is the transformed sound pressure, the wave number $k_m = k - k_x v_x/c - k_y v_y/c$ and the wave number $k_{mz}^2 = k_m^2 - k_x^2 - k_y^2$.

Since the wave number is constant in each layer (9) can be simplified before solving. After doing that and defining the boundary conditions, (9) can be solved stepwise from the ground surface and upwards (Salomons 2001).

As said above this basic form of the FFP has a major drawback since it cannot handle range-dependent atmosphere or ground. This also means that this FFP cannot include turbulence since that is a kind of range dependence. However, L'Espérance et al. (1995) have developed an alternative version of the fast field program called CERL-FFP which can include turbulence in a mildly refracting atmosphere. Also Raspet and Wu (1995) have to some extents managed to include turbulence in the FFP.

Quite recently a kind of range dependence has been made possible by combining the FFP with boundary element methods. The calculations are made stepwise in range and the boundary conditions between two steps are set to match each other. Schmidt et al. (1995) use such a combination of the FFP and boundary element methods to introduce range dependence for underwater acoustics. For atmospheric acoustics, Taherzadeh et al. (2001) have developed a similar method for predicting barrier effects.

5.2. The Parabolic Equation method

The PE method is another numerical method, or rather a family of methods, for calculating sound propagation. The solution is valid in the far field only. In the PE method, the approximation of the wave equation leads to a parabolic equation, hence its name. Two versions of the PE method will be described here: the Cranck-Nicholson PE (CNPE) and the Green's function PE (GFPE). The CNPE is the older of these two.

In the PE method, the sound field is calculated step-wise along the direction of propagation. This allows for including range dependence in both the atmospheric and the ground conditions. Robertson et al. (1996) have investigated long range, low-frequency sound propagation over impedance discontinuities with the PE method and found that it is well adapted to handle such cases.

In both the CNPE and the GFPE the ground surface is assumed to be flat. Small scale roughness can be incorporated directly into the model by modifying the surface impedance (see chapter 11.3). Large scale roughness such as a smooth undulating terrain can be taken into account by using the generalized terrain PE (GTPE) which is based on the CNPE. However, the angle restriction of the wide-angle PE still holds so the gradient of the terrain profile cannot be too steep (Sack and West, 1995).

5.2.1. Crank-Nicholson PE

For the CNPE, as for all PE methods, the sound speed and the ground conditions can vary with range. Axial symmetry is often assumed in sound propagation calculations. It means that only a plane in the x,z-domain is being studied; which reduces the calculation from a three-dimensional problem to a two-dimensional problem. PE methods can be used in three dimensions as well, though it would lead to quite time consuming calculations.

The original formulation of the CNPE was limited to quite small propagation angles, giving restrictions on the relation between the source and the receiver height. Later a so-called wide-angle PE was developed, which increased the possible propagation angle, but it is still restricted to around 30 degrees.

Thorough descriptions of the development of the CNPE can be found in Lee and McDaniel (1987) and West et al. (1992).

5.2.1.1. Low-angle CNPE

For the two-dimensional case, the starting point is the Helmholtz equation in two dimensions:

$$\frac{\partial^2 \Psi}{\partial x^2} + \frac{\partial^2 \Psi}{\partial z^2} + k^2 \Psi = 0 \tag{10}$$

where k is the wave number and $\Psi = p\sqrt{x}$ which includes the assumption of axial symmetry.

Introducing the operator Q as $Q = \partial^2/\partial z^2 + k^2$, and only considering outgoing waves yields:

$$\left(\frac{\partial}{\partial x} + i\sqrt{Q} \right) \Psi = 0 \tag{11}$$

for which a solution can be written as

$$\Psi(x,z) = \varphi(x,z) e^{ik_0 x} \tag{12}$$

where φ is the velocity potential (proportional to the sound pressure) which works like an envelope for the sound pressure. The wave number k_0 is a reference value which can be chosen as $k_0=\omega/c_0$, c_0 being a reference sound speed. The standard low-angle PE is obtained by inserting this into (10) and omitting second order deratives (West et al. 1992):

$$\frac{\partial \varphi}{\partial x} = i \left[\frac{1}{2k_0} \left(\frac{\partial^2}{\partial z^2} + (k^2 - k_0^2) \right) \right] \varphi \tag{13}$$

5.2.1.2. Wide-angle PE

Introducing another operator, q, as

$$q = \frac{1}{k_0}\left(\frac{\partial^2}{\partial z^2} + k^2\right) - \mathbf{1} = \frac{Q}{k_0^2} - \mathbf{1} \tag{14}$$

Now $\sqrt{Q} = k_0\sqrt{(\mathbf{1}+q}$. Expanding $\sqrt{\mathbf{1}+q}$ and omitting q^2 and higher powers of q will lead to equation (13). However, the wide-angle PE can be obtained by using a more accurate expansion:

$$\sqrt{\mathbf{1}+q} \cong \frac{\mathbf{1}+\frac{3q}{4}}{\mathbf{1}+\frac{q}{4}} \tag{15}$$

which is quadrically accurate in q and gives the wide-angle CNPE:

$$\left[\mathbf{1}+\frac{q}{4}\right]\frac{\partial\varphi}{\partial x} = ik_0\frac{q}{2}\varphi \tag{16}$$

5.2.1.3. Ground boundary condition

The surface impedance is equal to the ratio between the sound pressure and the normal particle velocity:

$$Z_s = \frac{p_0}{u_z} = \frac{p_0}{\frac{1}{i\omega\rho_s}\frac{\partial p}{\partial z}} \tag{17}$$

If the second order CNPE is used, the boundary condition should also be of second order. The second order finite form of (17) is (West et al. 1992):

$$Z_s = \frac{2i\omega\rho_s p_0 \Delta z}{4p_1 - 3p_0 - p_2} \tag{18}$$

5.2.1.4. Upper boundary condition

The upper boundary condition must be written so that the sound waves are not reflected back into the calculation region. This can be solved by creating an absorbing layer in the upper region where the absorption increases with height. This is suggested both by West et al. (1992) and Salomons (2001, p. 172).

At the top of the calculation grid a boundary condition is placed with an impedance of $Z_s = 1$. This impedance will cause vertically travelling plane waves to vanish. Waves that hit the surface with an angle will be somewhat reflected though, and these must be taken care of before reaching the essential parts of the calculation area. The absorbing layer in the upper part of the calculation grid will eliminate such reflected waves. The absorption is added as an imaginary term to the wave number:

$$k_a(z) = k(z) + iA_t \frac{(z - z_t)^2}{(z_M - z_t)^2} \qquad z_t \le z \le z_M \tag{19}$$

where $k_a(z)$ is the modified wave number, $k(z)$ the original wave number, A_t is a constant, z_t is the height where the absorbing layer begins and z_M is the top of the calculation area. A_t varies with frequency. According to Salomons (2001, p. 172), good results are obtained by choosing A_t=[1, 0.5, 0.4, 0.2] for f = [1000, 500, 120, 30] Hz.

The thickness of the absorbing layer must be chosen carefully. If the layer is too thin it will not remove all unwanted reflections while a too thick layer will unnecessarily increase the computation time. West et al. (1992) says that ten wavelengths is the minimum thickness while Salomons (2001, p. 172) says that fifty wavelength is on the safe side.

The height where the absorbing layer begins is also of importance. Salomons states that in a downward refracting atmosphere, the absorbing layer must be placed over the highest turning point of the sound rays. For an atmosphere with a typical logarithmic wind speed profile the maximum height of a sound ray is in the order of $h \approx 0.02r$ where r is the range (Salomons 2001, p. 172).

5.2.2. The Green's Function PE

The GFPE is an alternative formulation of the PE method. The GFPE can use longer calculation steps in the horizontal direction and is therefore faster than the CNPE. For the CNPE the maximum step size in both the horizontal and the vertical direction is a tenth of a wavelength while for the GFPE the step size in the horizontal direction can be as large as 50 wavelengths. The GFPE is on the other hand not as accurate as the CNPE for sound propagation with wide-angle propagation and large sound speed gradients (Salomons 2001, p. 164).

The GFPE starts with the Helmholtz equation in two dimensions:

$$\frac{\partial^2 q}{\partial r^2} + \frac{\partial^2 q}{\partial z^2} + k^2 q = 0 \tag{20}$$

where $q = p\sqrt{x}$ is the sound pressure taking axial symmetry into account, note that Salomons (2001) and West et al. (1992) use different annotations for this term. The atmosphere is as a first approximation assumed to be homogenous, non-refracting and unbounded; hence the wave number k is a constant. A Fourier transform is applied on (20) (Salomons 2001, p. 182):

$$\frac{\partial^2 Q}{\partial r^2} + (k^2 - k_z^2)Q = 0 \tag{21}$$

where

$$Q(r, k_z) = \int_{-\infty}^{\infty} e^{-ik_z z} q(r, z) dz \tag{22}$$

Equation (21) can be rewritten as

$$\left(\frac{\partial}{\partial r} - i\sqrt{k^2 - k_z^2}\right)\left(\frac{\partial}{\partial r} + i\sqrt{k^2 - k_z^2}\right)Q = 0 \qquad (23)$$

where the first term represents waves travelling in the positive r-direction and the second term represents waves travelling in the negative r-direction. The second term is omitted, since only forward-propagating waves are of interest. The first term has the solution (written in finite differential form):

$$Q(r + \Delta r, k_z) = Q(r, k_z)e^{i\Delta r\sqrt{k^2 - k_z^2}} \qquad (24)$$

An inverse Fourier transform of (24) yields:

$$q(r + \Delta r, z) = \frac{1}{2\pi}\int_{-\infty}^{\infty} e^{ik_z z}e^{i\Delta r\sqrt{k^2 - k_z^2}}Q(r, k_z)dk_z \qquad (25)$$

For an atmosphere that is bounded by an impedance plane the equation (25) will be more complicated. There will be three waves to take into account, the direct wave, the reflected wave and also a surface wave (Salomons 2001, p. 191).

5.2.2.1. The GFPE for refracting atmosphere

There are different ways to obtain the GFPE for a refracting atmosphere with a surface boundary. One of the formulations given by Salomons (2001, p. 191) will be described briefly here. Equation (20) can be rewritten as

$$\partial_r^2 q(r, z) = -H_2(z)q(r, z) \qquad (26)$$

where the operator $H_2(z) = k^2(z) + \partial_z^2$.

For one-way propagation:

$$\partial_r q(r,z) = iH_1(z)q(r,z) \tag{27}$$

where H_1 is another operator that satisfies $H_1^2 = H_2$. If the wave number is written as $k^2(z) = k_a^2 + \delta k^2(z)$ where k_a is a constant, equation (27) can be expressed as the sum of two terms:

$$\partial_r q(r,z) = iH_{1a}q(r,z) + i\frac{\delta k^2(z)}{2k_a}q(r,z) \tag{28}$$

where the first term represents the wave propagation in the corresponding non-refracting atmosphere and the second term is due to the effect of refraction. The finite difference form of (28) is obtained by integrating from r to r + Δr:

$$q(r+\Delta r,z) = e^{i\Delta r\frac{\delta k^2(z)}{2k_a}} e^{iH_{1a}\Delta r} q(r,z) \tag{29}$$

The first term in this expression is the refraction term. The GFPE for refracting atmosphere is hence obtained by multiplying the solution at each range step with a phase factor (Salomons 2001, p 192).

5.2.3. Incorporating turbulence in the PE-method

Since both the CNPE and the GTPE can handle range depending variations in the sound speed they are well fit to include turbulence. Salomons (2001, p. 221-229) gives a method of how to include turbulence in the PE-method by using the statistical properties of the fluctuating refraction index. The easiest and least time-consuming way to incorporate turbulence is to multiply the sound field with a phase factor at each range step. The value of this phase factor is determined from the appropriate turbulence spectrum (chapter 1.3).

5.3. Ray theory

Ray theory, or geometrical acoustics, is, unlike the FFP and the PE methods, an analytical method. The basic method consists of two steps; finding the sound rays that goes from the source to the receiver (ray tracing) and calculating the sound pressure at the receiver by adding the contributions from each ray. A sound ray follows a fundamental law called Fermat's principle. "Fermat's principle is that the actual ray path connecting $\mathbf{x}_A$ and $\mathbf{x}_B$ is such that it renders the travel-time integral T_{AB} stationary with respect to small virtual changes in the path." (Pierce 1991, p. 376) Fermat's principle is valid also for abrupt changes in the paths and predicts both the law of mirrors and Snell's law.

The ray tracing equations are given by Pierce (1991, p. 375):

$$\frac{d\mathbf{x}}{dt} = \frac{c^2\mathbf{s}}{\Omega} + \mathbf{v} \tag{30}$$

$$\frac{d\mathbf{s}}{dt} = -\frac{\Omega}{c}\nabla c - \mathbf{s}\times(\nabla\times\mathbf{v}) - (\mathbf{s}\bullet\nabla)\mathbf{v} \tag{31}$$

where $\mathbf{x}$ is the path of the ray, $\mathbf{v}$ is the velocity of the medium if it is in motion, $\mathbf{s}$ is the ray's slowness vector defined as $\mathbf{s} = \mathbf{n}/(c + \mathbf{v}\cdot\mathbf{n})$, $\mathbf{n}$ is the normal of the wave front and $\Omega = 1 - \mathbf{v}\cdot\mathbf{s}$.

For a stratified moving medium, Ostashev (1997, p. 73) expresses the ray tracing equations as

$$\frac{d\mathbf{r}}{d\tau} = \frac{\mathbf{a}}{k} + \frac{\mathbf{v}_\perp}{c} \tag{32}$$

$$\frac{dz}{d\tau} = \frac{q}{k} + \frac{v_z}{c} \tag{33}$$

where $\mathbf{r}$ is the horizontal path of the curve, $\mathbf{a}$ is the horizontal part of the wave vector, q is the vertical part of the wave vector, $\mathbf{v}_\perp$ is the horizontal velocity of the medium, v_z is the vertical velocity of the medium and k is the magnitude of the three-dimensional wave vector $k = (\mathbf{a}^2+q^2)^{1/2}$. By substituting (32) into (33) the ray path can be solved numerically.

When all rays from the source to the receiver have been found, the total sound pressure at the receiver can be calculated as the sum of the sound pressure (phase included) from each contributing ray:

$$p = \sum_m A_m e^{i\phi_m} \tag{34}$$

where

$$A_m = f_m C_m^{Nm} \tag{35}$$

is the amplitude of ray *m*, f_m is a focusing factor, C_m is the reflection coefficient of the ground and N_m is the number of reflections ray *m* has undergone. The phase of the ray is given by $\phi_m=\omega t_m$ where ω is the angular frequency and t_m is the travel time for the ray (Salomons 2001, p. 242). This way of adding contributions from single rays makes it possible to easily include the effects of turbulence. Since turbulence will cause variations in the sound pressure a fluctuating term is simply added to the sound pressure in (34). Hence

$$p_m = A_m e^{i\phi_m + \psi_m} \tag{36}$$

The term ψ_m is determined by the appropriate turbulence spectra (Salomons 2001, p. 260).

In ray theory, the sound amplitude of a ray is calculated by assuming that a certain amount of sound energy is passed along a tube surrounding the ray. The area of this tube is decided by the normal distance between two adjacent rays. At some points, for example where two rays intersect, the area of the tube goes towards zero, thus theoretically creating an infinite sound pressure at that point. These points form surfaces which are called caustics.

In reality, the sound pressure is high at caustic surfaces but not infinite. To obtain the real sound field, a caustic diffraction field needs to be added to the theoretical field. Another effect of caustics is that the rays touching a caustic surface undergo a phase shift of $-\pi/2$. Salomons (1998) have presented a ray tracing method that can handle caustics in an arbitrary downward refracting atmosphere. A thorough description of caustics as well as ray theory can also be found in Salomons (2001, app. L).

At long ranges and with the presence of wind and temperature gradients as well as a finite impedance ground it can be difficult to maintain a strictly geometrical approach to ray tracing. L'Espérance et al. (1992) have developed a method based on geometrical ray tracing often referred to as the heuristic model. The model takes refraction from a linear sound speed profile into account as well as geometrical spreading, absorption, ground effect and turbulence. The heuristic model has been shown to give good agreement with other propagation models at long ranges (Attenborough et al., 1995). It was believed that diffraction effects due to caustics were to distort the results at long ranges, but that seems not to be the case. Raspet et al. (1995) compared the heuristic model with FFP for long ranges using a realistic ground impedance. They also found good agreement and showed that the sound rays that are subject to strong caustic diffraction will be absorbed by the ground and can therefore not affect the result. The heuristic model has had quite a large impact on ray tracing since it was presented and several models based on or similar to the heuristic model has been developed since then (Li, 1996 and Li et al., 1998). It is also used in the Nordic Environmental Noise Predicion Methods; Nord2000 (Kragh et al. 2002).

6. Scattering models

Modelling scattering of waves by rough interfaces is of interest not only in acoustics but also in optics and more general electromagnetics. Even though the waves are very different in these fields, the wave theory remains the same in many aspects. In Ogilvy (1991), in-depth explanations of different scattering theories are given. Two of these (perturbation theory and Kirchhoff theory) are discussed in the beginning of this chapter since they deal with some of the fundamentals concerning scattering theory. In the latter part of the chapter some more acoustic-oriented scattering models are described.

6.1. Perturbation theory

The basis of all kinds of perturbation theory is to develop a model for a normal state and then make small additions (perturbations) to this state. In this case it means that the reflected field is calculated as if the surface was smooth and then adding perturbations. There are the following restrictions on the roughness of the surface and the wave number of the sound:

$$k \mid h(x,y) \mid << 1 \tag{37}$$

$$|\nabla h(x,y)| << 1 \tag{38}$$

where h(x,y) is a function describing the surface, ∇h(x,y) its gradient and k is the wave number (Ogilvy 1991, p. 39). The surface function h(x,y) is assumed to have a mean normal plane at z = 0. These restrictions mean that the height (or depth) of the roughness should be small compared to the wavelength (expressed as the wave number), and that the steepness of the roughness should be small compared to one.

In perturbation theory there are two commonly used boundary conditions, the Dirichlet and the Neumann boundary condition. The Dirichlet boundary condition is that the field is zero on the surface:

$$\Psi(r) = 0 \qquad \text{when } z = h \tag{39}$$

The reflected field is expanded as a sum of terms:

$$\Psi_{sc} = \Psi_0^{sc} + \Psi_1^{sc} + \Psi_2^{sc} + \Psi_3^{sc} + \cdots \tag{40}$$

Equation (40) shows the perturbation procedure, the term ψ_0^{sc} is in fact the reflected field in the case with a smooth surface (the coherent field) and the remaining terms are perturbation terms. Only considering terms of the first order, the first scattering term can be calculated as

$$\psi_1^{sc}(\mathbf{r}) = -\int_{S_M} h(\mathbf{r}_0)\left(\frac{\partial \psi^{inc}}{\partial z} + \frac{\partial \psi_0^{sc}}{\partial z}\right)\frac{\partial G(\mathbf{r},\mathbf{r}_0)}{\partial z_0} dS_M(\mathbf{r}_0) \tag{41}$$

where $G(r,r_0)$ is the half-space Green's function and S_M is the reflecting surface (Ogilvy 1991, pp 40-41).

If the surface mean height is zero, that is if $\langle h \rangle = 0$, the first scattering term will also have a zero mean value; $\langle \psi_1^{sc} \rangle = 0$. This is because the phase shifts are equally distributed so that the mean amplitude of the diffuse field will be zero. Hence, with this model, the coherent field will be the same as in the case of a smooth surface. On top of this there will be a diffuse field so, when calculating the intensity of the total reflected field, this model (to the first order) is not energy conserving. However, if the roughness is small, this error will be negligible. The intensity of the diffuse field is calculated as

$$\left\langle I_{(1)} \right\rangle = \left\langle \psi_1^{sc} \overline{\psi}_1^{sc} \right\rangle \tag{42}$$

where the second term in the parenthesis is the complex conjugate of ψ_1^{sc} (Ogilvy 1991, p. 41). Another suitable boundary condition is the Neumann boundary condition:

$$\frac{\partial \psi}{\partial n_0} = 0 \qquad \text{when } z = h \tag{43}$$

that is that the gradient of the field with respect to the surface normal, n_0, should be zero on the surface.

If the boundary condition is expressed in terms of rectangular coordinates, the expression for the field using the Neumann boundary condition will be more complicated than when using the Dirichlet boundary condition. However, the method of solving the problem is more or less the same. The reflected field is written as a sum of terms where term zero is the coherent field. This field will again not be affected by the rough surface; instead the roughness only creates an additional diffuse field. The roughness must therefore be small or the error caused by not conserving energy will be too large (Ogilvy 1991, pp. 43-46).

The accuracy of perturbation theory can be increased by using more terms in the expansion of the reflected field. Doing so will also to some extents include the effect of multiple reflections. Having said that, if the gradient of the surface (that is the steepness of the roughness) is small and the incoming angle of the sound also is small, perturbation theory to the first or second order is often accurate enough (Ogilvy 1991, pp. 59-63).

6.2. Kirchhoff theory

Ogilvy (1991, ch. 4) describes a method based on Kirchhoff theory that can be used to calculate the reflected field from a random rough surface. The method can be applied to roughness larger than $kh < kb << 1$ where h is the height of the roughness and b the distance between them, but the roughness must be smooth and the reflection must take place in the far field. Since it is assumed that the roughness is random, Ogilvy uses statistical methods to describe the surface. The calculated reflected field will therefore also be described by its statistics and the mean intensity is calculated rather than the exact value of the sound pressure amplitude.

The coherent and the diffuse field are calculated separately and later added to obtain the total field. The coherent field is obtained from the average amplitude of the scattered field. It can be calculated knowing the phase differences between the incoming and the reflected field (which depend on the surface statistics).

$$\left\langle \psi^{sc} \right\rangle = \frac{-ike^{ikr}}{4\pi r} 2F \int_{S_M} \int_{-\infty}^{\infty} e^{ik\phi(x_0,y_0)} p(h) dh dx_0 y_0 + \left\langle \psi_e \right\rangle \tag{44}$$

where $\langle \psi_e \rangle$ is the contribution from the edges of the reflecting surface, F is a coefficient depending on the angle between the incoming field and the surface (S_M), $\phi(x_0,y_0)$ is the phase function and p(h) the probability function of the surface (Ogilvy 1991, p. 85).

In the diffuse field the phase differences are such that the mean amplitude would be zero so instead, the mean intensity is calculated:

$$\begin{aligned} \left\langle I_d \right\rangle &= \left\langle \psi^{sc} \overline{\psi^{sc}} \right\rangle - \left\langle \psi^{sc} \right\rangle \left\langle \overline{\psi^{sc}} \right\rangle = \\ &= \frac{k^2}{(4\pi r)^2} 4F^2 \int_{S_M} e^{ik[A(x_0-x_1)+B(y_0-y_1)]} \times \left(\left\langle e^{ikC(h_0-h_1)} \right\rangle - \left\langle e^{ikCh_0} \right\rangle \left\langle e^{-ikCh_1} \right\rangle \right) dx_0 dx_1 dy_0 dy_1 \end{aligned} \tag{45}$$

where $\overline{\psi^{sc}}$ is the complex conjugate of the scattered field and A, B, C and F are coefficients that depend on the angle between the incoming field and the surface. These formulas are valid for a plane, monochromatic incoming wave ($\psi_{inc} = e^{i\mathbf{k}_{inc}\mathbf{i}}$). The reflection coefficient of the surface is assumed to be constant (Ogilvy 1991, p. 87).

If the surface is motionless, isotropic and has a Gaussian probability function, equation (44) and (45) leads to an exact analytical solution of the reflected field.

6.3. Boss theory

Boss theory applies to surfaces that can be described as a flat surface covered with a distribution of bosses (hemispheres, half-cylinders, half-ellipsoids etc). In boss theory, the roughness is included in the boundary condition most often as a modification of the surface impedance.

6.3.1. Early boss theory

Modern boss theory is mainly based on the parallel work done by Twersky and Biot during the 1950's and 1960's. They will be discussed here as an introduction to boss theory.

6.3.1.1. Twersky's work

Twersky developed a boss theory which yields an approximation of the power reflection coefficient and the phase change after the reflection for a random distribution of bosses on a rigid or free plane. His work is presented in a number of papers. Two different ways, depending on frequency, to calculate the variables stated above are presented by Burke and Twersky (1966).

Burke and Twersky (1966) give a general case where a plane wave is incident on a base plane, which has "uniformly random distribution of parallel arbitrary, identical cylindrical protuberances". The power reflection coefficient for the coherent field becomes:

$$R = \left|\frac{1+Z}{1-Z}\right|^2 = 1 + \frac{4\,\mathrm{Re}\,Z}{\left|1-Z\right|^2} \tag{46}$$

where

$$Z = \frac{n}{k\cos\varphi_0} f(\varphi_0, \pi - \varphi_0) \tag{47}$$

n is the average number of scattering elements per length and φ_0 is the direction of observation. For low frequencies, f is calculated as a sum of the scattering amplitude of a single protuberance, which will be correct to the eighth and sixth power of the real and the imaginary part of the frequency, respectively. For high frequencies, Burke and Twersky (1966) uses a "Kirchhoff-type" approximation.

The incoherent scattering in a direction φ is specified by the scattering cross-section, σ:

$$\sigma(\mathbf{s}, \mathbf{k}_i) = \sigma(\varphi, \pi - \varphi_0) = \frac{2n}{\pi k}\left|\frac{f(\varphi, \pi - \varphi_0)}{1-Z}\right|^2 \tag{48}$$

where $\mathbf{s} = \mathbf{i}\cos\varphi + \mathbf{j}\sin\varphi$.

When combining the coherent and incoherent fields the total reflected power, averaged over one period, is obtained:

$$\mathbf{P} = R(\mathbf{k}_0, \mathbf{k}_i)\mathbf{k}_0 + \int \left[\frac{\sigma(\mathbf{s}, \mathbf{k}_i)}{|\mathbf{r} - \mathbf{y}_s|} \right] \mathbf{s} dy_s \quad (49)$$

P is here normalised by the time-averaged incident power density, **s** is a unit vector as above, pointing from the point $\mathbf{y}_s$ on the plane to the observation point **r**.

The expressions for R and σ are approximations but follows expected behaviours like $R \rightarrow 1$ when $\varphi_0 \rightarrow \pi/2$. It is observed that the power reflection coefficient only depends on the boss dimension perpendicular to the reflected plane for high frequencies while it for low frequencies depends on the dimension in both directions (Burke and Twersky 1966).

6.3.1.2. Biot's work

At the same time, another boss theory was developed by Biot (1968). Biot represents the scattering by roughness as a boundary condition and after expressing this boundary condition the surface can be regarded as smooth. It is valid for roughness small compared to a wavelength. Except for that condition, the roughness can have arbitrary shape and distribution over the surface.

The scattered field is represented as a continuous distribution of sources and dipoles (sources = monopoles). Biot considers first the case where the scatterer is a single solid sphere of radius a. The scattered field can be represented as the sum of the fields from a dipole and a monopole .The dipole field has the velocity potential φ_d:

$$\varphi_d = -\left(\frac{1}{2}\right) a^3 \mathbf{U}_0 \cdot \nabla F \quad (50)$$

where $\mathbf{U}_0$ is the velocity of the incident wave at the origin, $F = e/R^{-ikR}$ and $R = (x^2+y^2+z^2)^{1/2}$.

The monopole field has the velocity potential φ_s:

$$\varphi_s = (1/3)a^3 D_0 F \tag{51}$$

where $D_0 = \nabla \cdot \mathbf{U}$ and $\mathbf{U}$ is the velocity field of the incident wave in the absence of the sphere. The total scattered field is the sum of the dipole and the monopole. It is shown by Biot (1968) that these two terms are of the same order and both must therefore be considered.

As said above, a rough surface can be represented by a distribution of monopoles and dipoles over the surface and this distribution of sources can be included in a boundary condition. According to Biot the boundary condition will be $\partial\phi/\partial z = \partial\phi_s/\partial z$ (for a smooth surface the corresponding boundary condition is $\partial\phi/\partial z = 0$). ϕ_s is the velocity potential for the total field scattered by a rough surface and

$$\frac{\partial \phi}{\partial z} = \frac{\partial \phi_s}{\partial z} = -2\pi\left(\frac{\partial \mu_x}{\partial x} + \frac{\partial \mu_y}{\partial y}\right) - 2\pi\mu \tag{52}$$

Here μ_x and μ_y are the densities of the dipole magnitudes and μ is the density of the monopole magnitude. These densities are what must be determined from the properties of the rough surface.

If the bosses on a rough surface are closely packed, the scattered field from the individual bosses will interact with each other, which must be taken into account. It is mainly the field from the dipoles that interact. Biot introduces a coefficient $\kappa = 1+\pi^2a^3/4b^3$ where a is the size of the bosses and b the distance between them. It is obvious that this term quickly goes towards 1 as b increases. κ is included in the formulas by $\mu_x' = (1/\kappa)\mu_x$ and $\mu_y' = (1/\kappa)\mu_y$ where μ_x' and μ_y' are the dipole densities corrected for the interference between the dipoles.

Different boss shapes will of course affect the scattered field. A shape factor σ is therefore introduced where $\sigma = 1$ for hemispherical bosses, $\sigma > 1$ for sharp roughness and $\sigma < 1$ for flat roughness. The shape factor is included in the dipole densities as $\mu_x' = \sigma\mu_x$ and $\mu_y' = \sigma\mu_y$. In a similar manner, Biot's model can also easily include the effects of non-uniform roughness where the boss density, spacing or shape varies over the surface.

Biot (1968) also shows that the roughness can induce a surface wave, which propagates along the surface and dies out exponentially away from the surface (see chapter 4.2.1).

6.3.2. Modern boss theory

Tolstoy (1984) has expanded the theories of Biot for low-frequency scattering. Tolstoy also gives a description of Twersky's boss model (which is valid also outside the low-frequency domain) but thinks that it is over-elaborate for the low-frequency case and, most importantly, cannot include scattering motion.

The low-frequency constraint of Tolstoy's boss model is: $kb \cong kh \leq 1$. That is that the height of the bosses (b) as well as the distance between them (h) should be small compared to the wavelength. The boundary condition used in this domain is

$$\frac{\partial \phi_s}{\partial z} = \eta \phi \tag{53}$$

where ϕ_s is the potential of the scattered field and ϕ is the total acoustic potential (if ϕ_0 is the velocity potential of the field in the absence of roughness $\phi = \phi_0 + \phi_s$). The main problem here is to determine η which Tolstoy (1984) does for some different kinds of boss shapes.

Medwin et al. (1984) compares Tolstoy's theories with experiment. They find good agreement for closely packed spherical and cylindrical bosses. However, with steep-sloped roughness elements and when the bosses are separated, there are significant differences between theoretical values and measurement results. Boulanger et al. (1998) find that Twersky's theories are more complete than Tolstoy's and that they include the effects of incoherent scattering and interactions between the scatters. Boulanger et al. generalise Twersky's semi-cylindrical theory to include other geometrical forms like triangular bosses and bricks. The general form for the surface admittance is

$$\beta = \eta - i\xi \tag{54}$$

where the imaginary part ξ is constant for all forms.

$$\xi = kV\left[-1+\left(\delta\cos^2\varphi+\sin^2\varphi\right)\sin^2\alpha\right]+O(k^3) \tag{55}$$

where k is the wave number, V is the raised cross-sectional area of the bosses, φ is the horizontal angle between the normal axis of the bosses and the propagation direction, α is the angle of the incoming sound wave (α=π/2 for grazing incidence) and δ is a measure of the dipole coupling which depends on the shape of the bosses (Boulanger et al. 1998).

The real part, η, is zero for periodic scattering. Otherwise it depends on the shape of the bosses. For semi-cylinders η becomes

$$\eta(\alpha,\beta)=\frac{nk^3\pi^2a^4}{8}\left(1-W^2\right)\left\{\left(1-\sin^2\varphi\sin^2\alpha\right)\left[1+\left(\frac{\delta^2}{2}\cos^2\varphi-\sin^2\varphi\right)\sin^2\alpha\right]\right\}+O(k^5) \tag{56}$$

where n is the number of bosses per unit length, a is the radius of the semi-cylinders and the term ($1-W^2$) is a packing factor for randomly distributed bosses. W = b*/b where b* is the minimum period and b is the mean period of the bosses. For triangular and semi-elliptical bosses:

$$\eta(\alpha,\beta)=\frac{k^3bV^2}{2}\left(1-W^2\right)\left\{\left(1-\sin^2\varphi\sin^2\alpha\right)*\left[1+\left(\frac{\delta^2}{2}\cos^2\varphi-\sin^2\varphi\right)\sin^2\alpha\right]\right\}+O(k^5) \tag{57}$$

where b is the base of the triangle or semi-ellipse. (Note the difference to Tolstoy who uses b as the height of the bosses.) The theory is compared with measurements and good agreement is found for small wooden slats and rods (Boulanger et al. 1998).

So far, all the theories considered here have been concerned with hard surfaces. Attenborough and Waters-Fuller (2000) expand the theories of Twersky and Tolstoy for surfaces with finite impedance. The basis is Tolstoy and Biot's expression for the surface admittance but results from Twersky are also used to include incoherent scattering.

The normalised surface admittance becomes:

$$\beta^* = \eta - ik_0 \cos^2(\varphi)\varepsilon^*_{01} + \beta \tag{58}$$

and

$$\eta(\alpha,\varphi) \approx \frac{k_0^3 b V^2}{2}(2 - W^2) * \cdots \cdots \left\{ (1 - \sin^2\alpha \sin^2\varphi)\left[1 + \left(\frac{\delta^2}{2}\cos^2\varphi - \sin^2\varphi \right)\sin^2\alpha \right] \right\} + O(k_0^5) \tag{59}$$

where ε_{01} is a factor depending on the cross-sectional area V, the densities of the atmosphere and the ground and the shape of the bosses, β is the normalised admittance for the corresponding smooth surface. Other variables are defined according to equation (56) and (57). The model is valid for bosses that are small compared to a wavelength, such as $kh < kb << 1$. Theoretical calculations are compared with measurements in the paper and they show fairly good agreement (Attenborough and Waters-Fuller 2000).

Tolstoy (1984) compares the boss theory with perturbation theory, saying that perturbation theory is useful when the exact contours of the surface is not known, only its statistics, and it is valid for both low and high frequencies. It is restricted though, to random, gently undulating roughness. Hence there are restrictions not only on roughness size but also on the steepness of the roughness.

6.4. Boundary element integrals

In the paper by Boulanger et al. (1998) they use a boundary integral equation method (BIE) by Chandler-Wilde and Hothersall (1985) for roughness that exceeds the domain $kh < kb << 1$. The BIE is originally developed for flat surfaces with varying impedance but can be used for rough surfaces as well though the discretisation of the surface must be finer than for a corresponding flat surface.

The BIE method begins with the inhomogeneous Helmholtz equation for an acoustic field above an impedance plane:

$$(\nabla^2 + k^2)\phi(\mathbf{r}) = f(\mathbf{r}) \tag{60}$$

where $\phi(\mathbf{r})$ is the velocity potential. The boundary conditions are the ground surface and the Sommerfeld radiation condition:

$$\frac{\partial\phi(\mathbf{r})}{\partial n} = ik\beta(\mathbf{r})\phi(\mathbf{r}) \tag{61}$$

$$\lim r \to \infty, \quad r^{\varepsilon}\left(\frac{\partial\phi}{\partial r} - ik\phi\right) = 0 \tag{62}$$

where n is the normal to D, β is either 0 (for a rigid surface) or Re β > 0 (for a locally reacting surface) and ε is ½ for two-dimensional and 1 for three-dimensional sound propagation. The solution for this boundary problem can be expressed by the following integral:

$$\phi(\mathbf{r}) = \phi_0(\mathbf{r}) - \int_{\partial D}\left(G(\mathbf{r},\mathbf{r}_0)\frac{\partial\phi(\mathbf{r}_0)}{\partial n(\mathbf{r}_0)} - \phi(\mathbf{r}_0)\frac{\partial G(\mathbf{r},\mathbf{r}_0)}{\partial n(\mathbf{r}_0)}\right)dS(\mathbf{r}_0) \tag{63}$$

and

$$\phi_0(\mathbf{r}) = \int_D f(\mathbf{r}_0)G(\mathbf{r},\mathbf{r}_0)dV(\mathbf{r}_0) \tag{64}$$

where ∂D is the surface and $G(r,r_0)$ is the Green's function to the corresponding source (line or point source) at r_0 (Chandler-Wilde and Hothersall, 1985). The surface ∂D can now be divided into segments of different surface impedances or different surface elevations (Boulanger et al. 1998).

Part II

7. Method

7.1. Calculation model

The calculation model developed in this project is the wide-angle CNPE such as it is described by West et al. (1992) with some adjustments; the upper and lower boundary conditions are somewhat differently expressed as well as the formulation of the source. These adjustments all follow Salomons (2001, App G).

The ground boundary condition is of second order using the normalised surface impedance (Salomons 2001, p. 171):

$$p_0 = \left(3 - 2ik_0 \frac{\Delta z}{Z}\right)^{-1} (4p_1 - p_2) \tag{65}$$

where Δz is the step size in the vertical direction and p_0, p_1 and p_2 are the sound pressure in three subsequent calculation points. The upper boundary condition is set as thick as fifty wavelengths as advised by Salomons (2001, p. 172). This is probably more than enough but due to the long calculation ranges even minor reflections from the upper boundary might accumulate and create significant errors, so, it is seems best to be on the safe side when it comes to the thickness of the absorbing layer. The absorbing layer is described by:

$$k_a(z) = k(z) + iA_t \frac{(z - z_t)^2}{(z_M - z_t)^2} \qquad z_t \le z \le z_M \tag{66}$$

where A_t is a frequency-dependent constant. Here $A_t = 0.242$ (Salomons 2001, p. 172).

The starting field is a unit point source located at the source height z_s.

$$q(0,z) = q_0(z - z_s) + Cq_0(z + z_s) \tag{67}$$

where:

$$q_0(z) = \sqrt{ik_0}(A_0 + A_2 k_0^2 z^2) e^{\left(-\frac{k_0^2 z^2}{B}\right)} \tag{68}$$

A_0 = 1.3717, A_2 = -0.3701 and B = 3 are constants. C = (Z-1)/(Z+1) is the reflection coefficient and k_0 is the vertical wave number which is assumed to be constant (Salomons 2001, pp 178-179).

Having expressed the boundary conditions, the starting field and knowing the sound speed profile, the finite form of the wide-angle CNPE can be expressed. First, the wide-angle PE, equation (16), is repeated:

$$\left[\mathbf{1} + \frac{q}{4}\right]\frac{\partial \varphi}{\partial x} = ik_0 \frac{q}{2}\varphi \tag{69}$$

The expression within the brackets in equation (69) is restated as

$$\left(\mathbf{1} + \frac{q}{4}\right) \equiv \left[\mathbf{1} + \frac{\mathbf{E}}{2ik_0}\right] \tag{70}$$

for which $\mathbf{E} = a\mathbf{T} + \mathbf{D}$ where:

$$a = \frac{i}{2k_0 \Delta z^2} \tag{71}$$

T is a sparse matrix:

$$\mathbf{T} = \begin{pmatrix} -2+s_1 & 1+s_2 & & \\ 1 & -2 & 1 & \\ & 1 & -2 & 1 \\ & \ddots & \ddots & \ddots \end{pmatrix} \tag{72}$$

Where s_1 and s_2 introduce the ground boundary condition:

$$s_1 = \frac{4}{3-2ik_0\frac{\Delta z}{Z}} \quad \text{and} \quad s_2 = -\frac{1}{3-2ik_0\frac{\Delta z}{Z}} \tag{73}$$

An equivalent boundary condition is placed at the top of the calculation grid with Z = 1. **D** is a diagonal matrix:

$$\mathbf{D} = diag(b_1, b_2, b_3 ...) \tag{74}$$

where

$$b_m = \frac{i(k_m^2 - k_0^2)}{2k_0} \tag{75}$$

is the variable that introduces refraction. Two matrices, **M1** and **M2**, are created as:

$$\mathbf{M}_1 = \mathbf{1} + \mathbf{E}\frac{\Delta x}{2} + \frac{\mathbf{E}}{2ik_0} \quad \text{and} \quad \mathbf{M}_2 = \mathbf{1} - \mathbf{E}\frac{\Delta x}{2} + \frac{\mathbf{E}}{2ik_0} \tag{76}$$

Now the finite difference form of the sound field can be expressed:

$$\mathbf{M}_2\varphi(x+\Delta x) = \mathbf{M}_1\varphi(x) \tag{77}$$

The result of the PE model is the sound pressure "envelope" term φ at each point in the calculation grid. To obtain the pressure, φ is divided by the square root of the distance to the source ($\sqrt{x}$) (which takes into account geometrical spreading in the horizontal range) and multiplied with the source strength (in this case the source strength is one, so this term is omitted). The relative sound pressure level is calculated as

$$L_p = 20\log\left(\frac{|p|}{|p_0|}\right) \tag{78}$$

where p_0 is the sound pressure one calculation step away from the source (West et al., 1992).

7.2. Impedance model

To include the roughness of the water waves, the boss model suggested by Boulanger et al. (1998) is used. The semi-elliptical boss profile or the triangular profile seems to be the best representation of a water surface since they can be expanded in width in a way a semi-cylindrical profile cannot. The impedance of a surface is: $Z = (1/\beta) = 1/(\eta + \xi i)$. For a surface covered with triangular or semi-elliptical bosses the real and the imaginary part of the relative admittance, β, become:

$$\eta(\alpha,\beta) = \frac{k^3 b V^2}{2}\left(1-W^2\right)\left\{\left(1-\sin^2\varphi * \sin^2\alpha\right) * \left[1+\left(\frac{\delta^2}{2}\cos^2\varphi - \sin^2\varphi\right)\sin^2\alpha\right]\right\} + O(k^5) \tag{79}$$

$$\xi = kV\left[-1+\left(\delta\cos^2\varphi + \sin^2\varphi\right)\sin^2\alpha\right] + O(k^3) \tag{80}$$

where α is the angle of the incoming sound wave (α=π/2 for grazing incidence), φ is the horizontal angle between the normal axis of the bosses and the propagation direction, k is the horizontal wave number, b is the period of the bosses, V is the raised cross-sectional area of the bosses, $(1-W^2)$ s a packing factor and δ is a measure of the dipole coupling which depends on the shape of the bosses (Boulanger et al., 1998).

The dimensions of the bosses are chosen to resemble the wave conditions of the Baltic Sea. According to Mårtensson and Bergdahl (1987) the mean wave height at Ölands Södra Grund and Hoburg is 1 m and the mean period is 4 s. Using equation (3) and (4) this corresponds to a wavelength of about 25 m for deep water conditions and somewhat more for shallow waters.

A Fourier analysis has been made to relate the height of the bosses with the height of the water waves. The amplitude of the first cosine term in the Fourier expansion is assumed to correspond to half the wave height. This is, of course, a simplification but the method still gives realistic results. One-metre high waves correspond to semi-ellipses of 0.89 m and triangles of 1.25 m height.

The profile geometry is shown in figure 15. If nothing else is stated, the properties of the surface profiles are as defined in table 3. The period of the profiles is assumed to vary randomly.

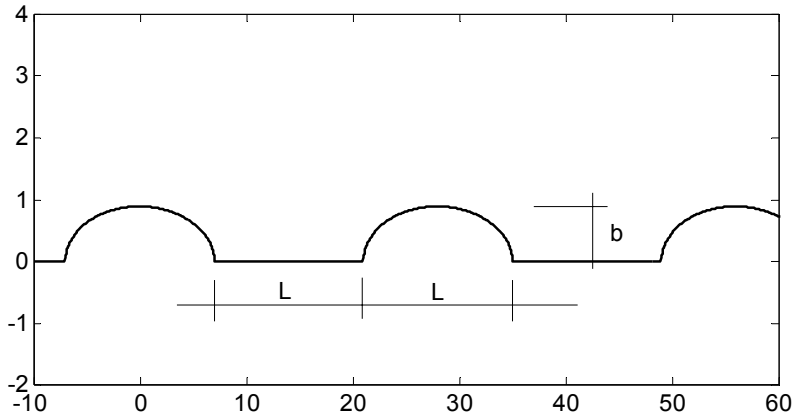

Figure 15 Geometry of the semi-elliptical boss profile.

Surface name	*Height (b)*	*Base (L)*	*Mean period (2L)*	*Min period (1.8L)*
Semi-elliptical	0.89 m	14 m	28 m	25.2 m
Triangular	1.25 m	14 m	28 m	25.2 m

Table 3 Definition of surface profiles.

It should be noted that the boss model by Boulanger et al. (1998) has a low-frequency constraint. The height of the roughness (b) must be small compared to a wave length such as kb < 1. This gives that the semi-elliptical boss profile of height 0.89 m is valid for frequencies below 60 Hz and the triangular profile of height 1.25 m is valid for frequencies below 43 Hz. Using the triangular boss profile for 50 Hz is to exceed the limitation of the model slightly. The semi-elliptical boss profile is therefore used in most of the calculations.

Calculations are also made using natural ground surfaces. The impedance model suggested by Embleton et al. (1983) is used for surfaces with flow resistivity of σ = 50 rayls (which corresponds to a forest floor) and for σ = 500 rayls (hard grass surface).

$$Z = 1 + 9.08\left(\frac{f}{\sigma}\right)^{-0,75} + 11.9i\left(\frac{f}{\sigma}\right)^{-0,73} \quad (81)$$

The impedance of the surfaces used is shown in table 4.

Surface	*Impedance*	*Equation*
Flat, totally reflecting	Infinite	
Semi-elliptical	172.92070 + 108.74228i	(79) & (80)
Triangular	50.600603 +24.030437i	(79) & (80)
Forest floor	10.0800 +11.9000i	(81)
Grass surface	52.0606+63.9068i	(81)

Table 4 Calculated impedances at 50 Hz of the different surface types used in the calculations.

7.3. Sound speed profile

The model includes the effect of refraction by using the effective sound speed. Calculations are made for a logarithmic wind profile with varyingly strong refraction and a low level jet constructed after measurements by Källstrand (1998).

The sound speed profiles with logarithmic wind are expressed as:

$$c(z) = c_0 + b\ln\left(1 + \frac{z}{z_0}\right) \tag{82}$$

where c_0 is the nominal sound speed set to 340 m/s, b is a refraction constant and z_0 is a reference height. Note that (82) differs slightly from (1) and that z_0 in this case does not correspond to the surface roughness parameter.

Using b = 2.5 m/s and z_0 = 0.5 m leads to a wind speed of 8 m/s at 10 m height, which is roughly the mean wind speed at Ölands Södra Grund and Hoburg (see chapter 3.3.1). This profile is therefore used to represent normal conditions for the Baltic Sea.

The low level jet profile is defined step-wise:

$$\begin{aligned}
c(z) &= c_0 + b\ln\left(1 + \frac{z}{z_0}\right) && (0 \le z \le 100)) \\
c(z) &= c_{100} + \frac{1}{10} * (z - 100) && (100 < z \le 200) \\
c(z) &= c_{200} && (200 < z \le 250) \\
c(z) &= c_{250} - \frac{7}{150} * (z - 250) && (250 < z \le 400) \\
c(z) &= c_{400} + \frac{1}{800} * (z - 400) && (z > 400)
\end{aligned} \tag{83}$$

where b = 1 m/s and z_0 = 0.5 m. The sound speed profiles used in the calculations are defined in table 5.

Profile name	*Description*
Profile 1 – weak refraction	Logarithmic profile; z_0 = 0.5, b = 1.0
Profile 2 – normal refraction	Logarithmic profile; z_0 = 0.5, b = 2.5
Profile 3 – strong refraction	Logarithmic profile; z_0 = 0.5, b = 5.0
Profile 4 – low level jet	See equation 83
Profile 5 – over land	Logarithmic profile; z_0 = 1.0, b = 1.0
Profile 6 – modified LLJ	See equation 84

Table 5 Sound speed profiles used in the calculations.

Profiles 2, 4 and 6 are shown in fig 16.

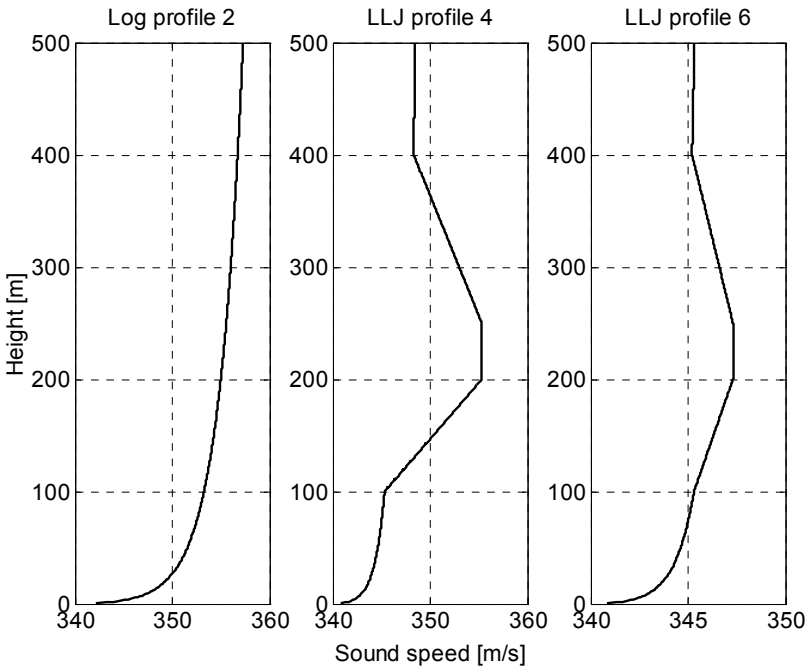

Figure 16 Sound speed profiles used in the calculations. From the left a logarithmic profile with b = 2.5 m/s, z_0=0.5 m (profile 2), a profile with a low level jet (profile 4) and finally a profile with a modified LLJ (profile 6).

7.4. Shore line

For the first set of calculations the atmospheric and the ground boundary conditions are assumed to be constant. For the second set of calculations a shoreline is introduced. Calculations with a shore are made for both logarithmic and low level jet sound speed profiles over the sea (profile 1, 2 and profile 4). Over land a logarithmic sound speed profile is assumed as defined in equation (82) with b = 1 m/s and z_0 = 1.0 m (profile 5).

For the case with a logarithmic wind over both the sea and over land, the sound speed profile and the ground properties are changed at the shore line. For the case with a low level jet over the sea the sound speed profile is changed in two steps. At the shore line a modified LLJ profile is assumed (defined in equation (84)). 500 m inland, the profile is changed to the logarithmic inland profile (profile 5). The ground boundary condition is changed at the shore line.

$$
\begin{aligned}
c(z) &= c_0 + b\ln\left(1+\frac{z}{z_0}\right) && (0 \le z \le 100)) \\
c(z) &= c_{100} + \frac{1}{50} * (z-100) && (100 < z \le 200) \\
c(z) &= c_{200} && (200 < z \le 250) \\
c(z) &= c_{250} - \frac{7}{500} * (z-250) && (250 < z \le 400) \\
c(z) &= c_{400} + \frac{1}{800} * (z-400) && (z > 400)
\end{aligned}
\qquad (84)
$$

with b = 1.0 m/s and z_0 = 1.0 m.

7.5. Validation of the model

The model has been tested against benchmark cases defined by Attenborough et al. (1995) and show good agreement with these. Case 2, downward refraction with a sound speed gradient of +0.1 s^{-1} and a constant surface impedance of Z = 12.81+11.62i, is shown in figure 17 and 18. The frequency is 100 Hz.

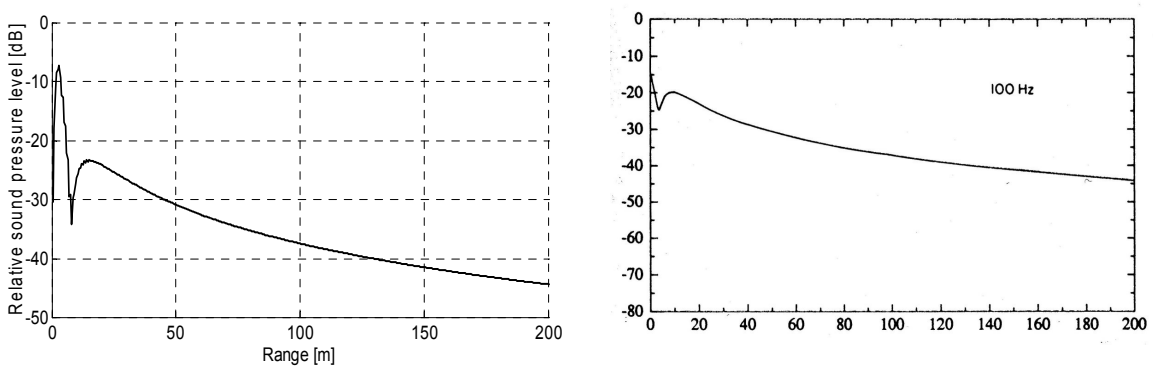

Figure 17 Calculations (to the left) compared with benchmark case 2 for 100 Hz by Attenborough et al. (1995) (to the right).

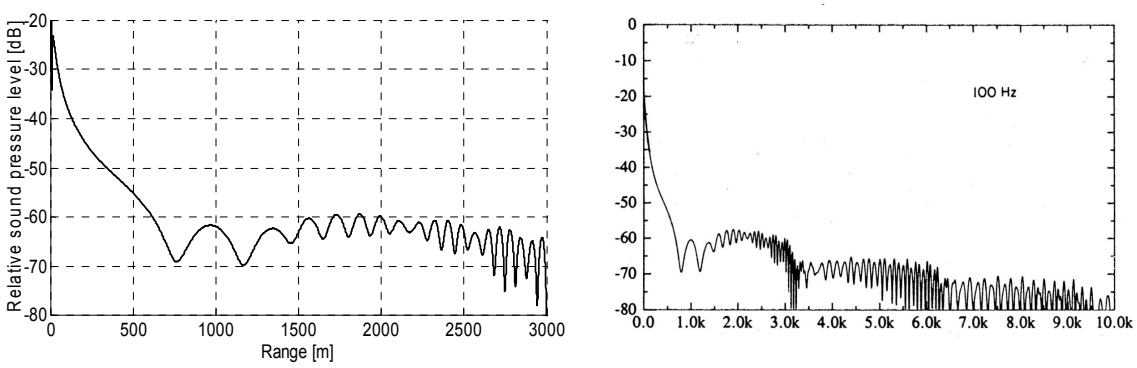

Figure 18 Calculations (to the left) compared with benchmark case 2 for 100 Hz by Attenborough et al. (1995) (to the right). Note the difference in range.

The long range calculation (figure 18) was terminated at 3000 m since further calculations under these conditions made the program run out of memory.

8. Calculations

The following quantities are used in all calculations (unless else is stated):

frequency:	50 Hz
source:	unit point source according to equation (67)
source height:	65 m
calculation step size:	2/3 m
calculation grid:	650 x 8110 m

Absorption and turbulence are not included in the calculations.

As explained in the previous chapter, the result from the calculations is the sound pressure level relative to the sound pressure level one calculation step away from a point source. Using a step size of 2/3 m, this corresponds to a source with a sound power level of $10\log(4\pi) + 20\log(2/3) = 7.5$ dB.

The coding is made in Matlab and an example code can be found in Appendix 1. Using a computer with a 2.4 GHz Pentium IV processor, the calculations take about 10 minutes for homogenous conditions and somewhat longer for calculations with a shore line. It should be noted that little effort has been made to optimise the code and it is possible that the calculation time can be reduced.

8.1. Varying surface properties

First, the difference in relative sound pressure level between a flat, totally reflecting surface, the semi-elliptical and the triangular boss surfaces is investigated. As can be seen in figure 19 the sound pressure level is almost identical for the flat surface and the semi-elliptical boss surface. The triangular boss profile gives slightly lower sound pressure levels, which is expected since the bosses have a higher profile; hence the impedance is lower. The same behaviour can be seen if comparing the flat surface with several semi-elliptical boss surfaces with varying height of the bosses (figure 20). A logarithmic sound speed profile with weak refraction (profile 1) has been used in these calculations to give attention to the differences between the surfaces.

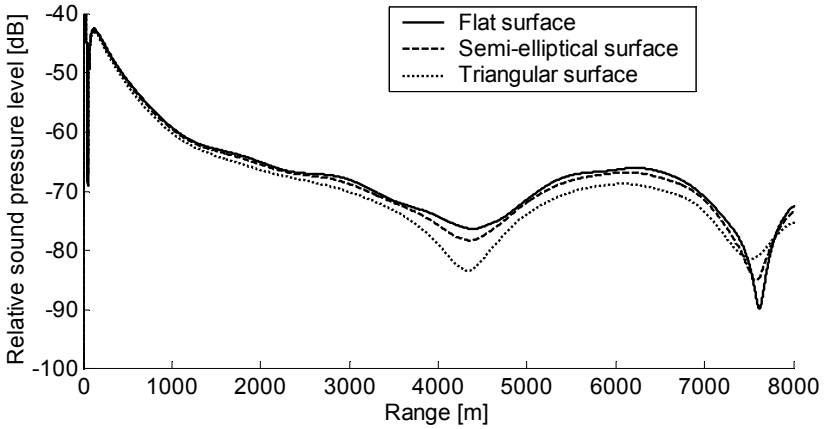

Figure 19 Relative sound pressure level calculated for a flat, totally reflecting surface (infinite impedance), the semi-elliptical boss surface (Z = 172.92070 + 108.74228i) and the triangular boss surface (Z = 50.600603 +24.030437i). The sound speed profile is logarithmic with weak downwards refraction (profile 1) and the receiver height is 1.33m.

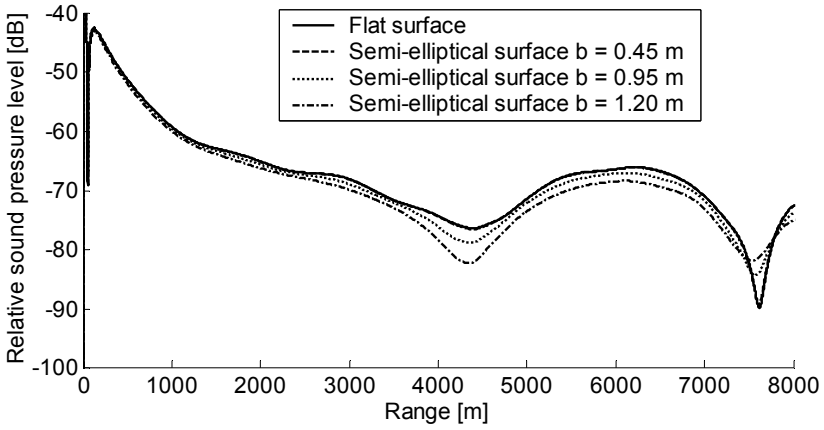

Figure 20 Relative sound pressure level calculated for different semi-elliptical boss surfaces with increasing height. The receiver height is 1.33 m and there is a logarithmic sound speed profile with weak downwards refraction (profile 1).

These results indicate that water waves that are small compared to the wave length of the sound (1 m or less for 50 Hz) have little impact on the sound pressure level.

The sound pressure level maximum at about 6000 m range is a result of interference. This becomes clear when comparing calculations at 50 Hz, 40 Hz and 20 Hz (figure 21). The same step size (2/3 m) has been used in all three calculations.

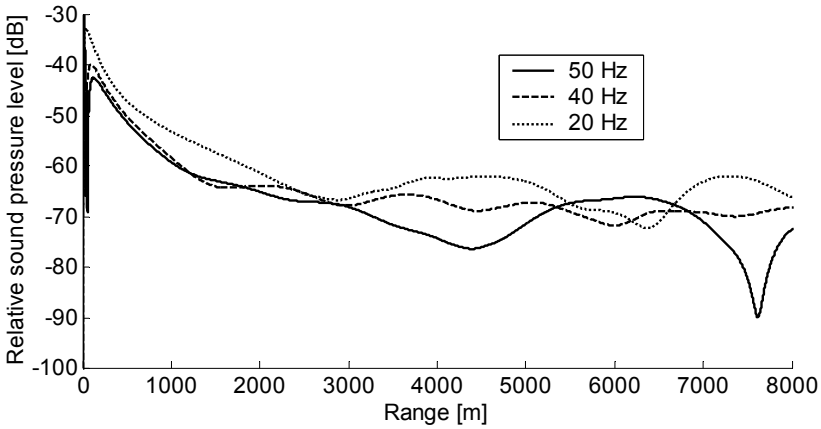

Figure 21 Relative sound pressure level calculated for a flat, totally reflecting surface at 50 Hz, 40 Hz and 20 Hz. The receiver height is 1.33 m and there is downwind conditions using a logarithmic sound speed profile with weak downward refraction (profile 1).

For a sound source emitting a pure tone, the locations of the sound pressure level maxima and minima due to interference are of great importance. However, for a broadband sound source the effects of interference are reduced since these maxima and minima will be at different places for different frequencies.

Calculations are also made for natural ground surfaces. Figure 22 shows a comparison between a flat, totally reflecting surface, the semi-elliptical boss surface and two natural ground surfaces.

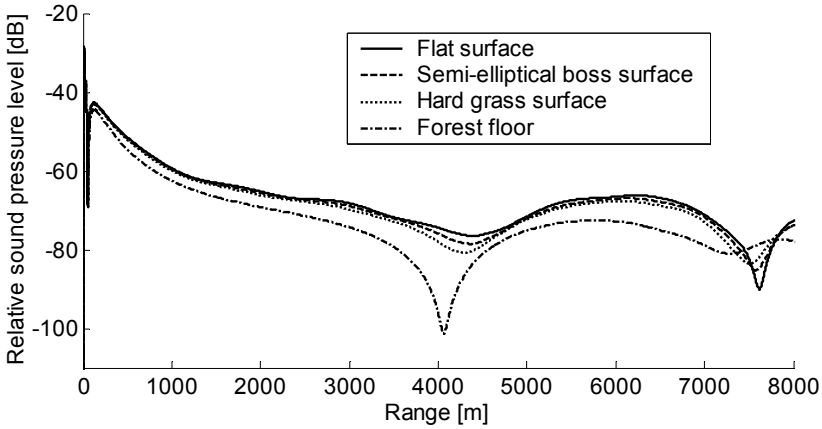

Figure 22 Relative sound pressure level calculated for a flat, totally reflecting surface, the semi-elliptical boss surface (Z = 172.92070 + 108.74228i), a flat, hard, grass surface (Z = 52.0606+63.9068i) and a forest floor (Z = 10.0800 +11.9000i). The sound speed profile is logarithmic with weak downward refraction (profile 1) and the receiver height is 1.33m

A colour plot of the calculation area for the totally reflecting surface, the semi-elliptical boss surface and the forest floor surface can be seen in figure 23, 24 and 25 respectively. Note that the angle restriction of the wide-angle CNPE gives unrealistic results in the upper left part of the calculation area.

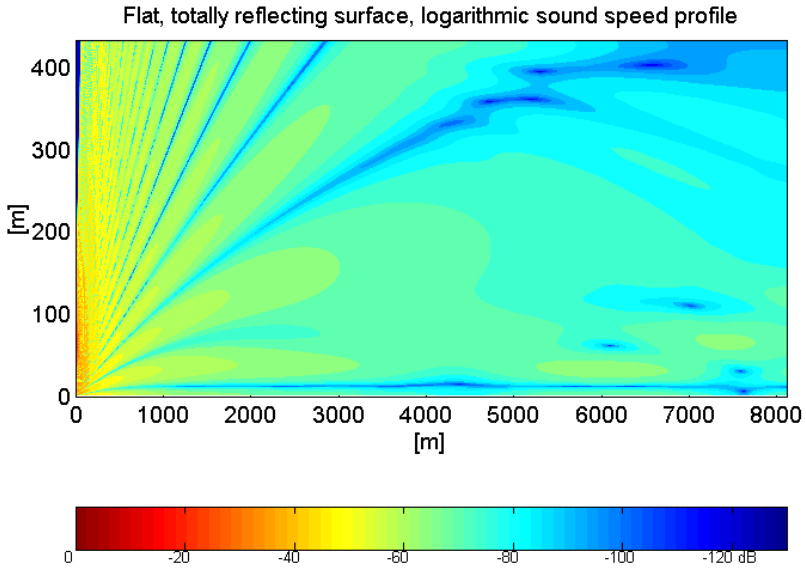

Figure 23 Calculation of the relative sound pressure level for a weak downwards refracting atmosphere (profile 1) and a flat, totally reflecting surface (infinite impedance).

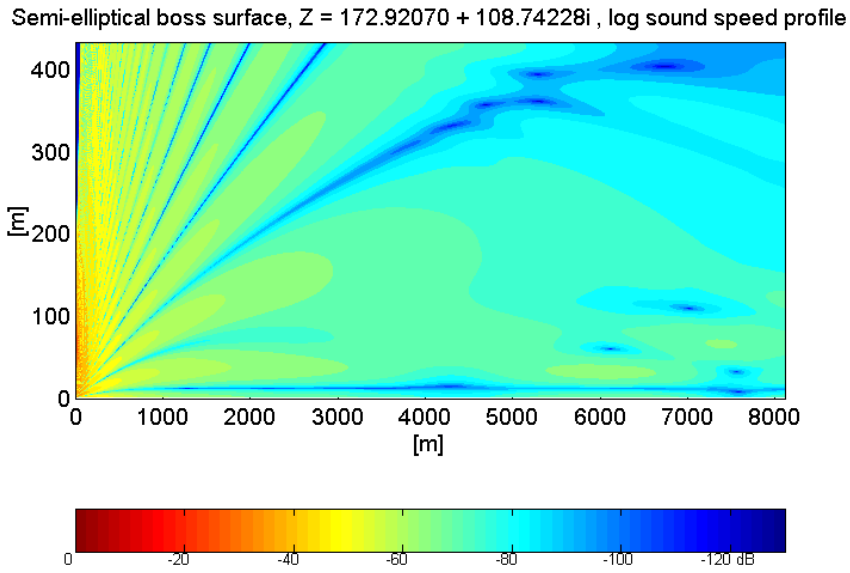

Figure 24 Calculation of the relative sound pressure level for a weak downwards refracting atmosphere (profile 1) and the semi-elliptical boss surface.

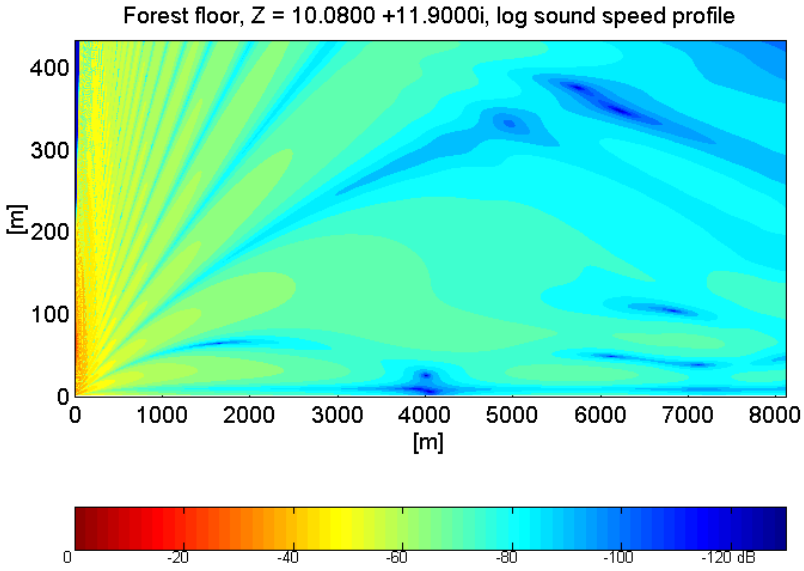

Figure 25 Calculation of the relative sound pressure level for a weak downwards refracting atmosphere (profile 1) and a forest floor surface.

As can be seen in figure 23 to 25, the different surfaces yield rather similar results even though the sound pressure level is decreasing somewhat faster in figure 25 due to the lower impedance of that surface.

Looking carefully, figure 23 to 25 all show a concentration of sound near the ground surface. This is even clearer in figure 26 that depicts the sound pressure level in the lower part of the atmosphere at different ranges from the source.

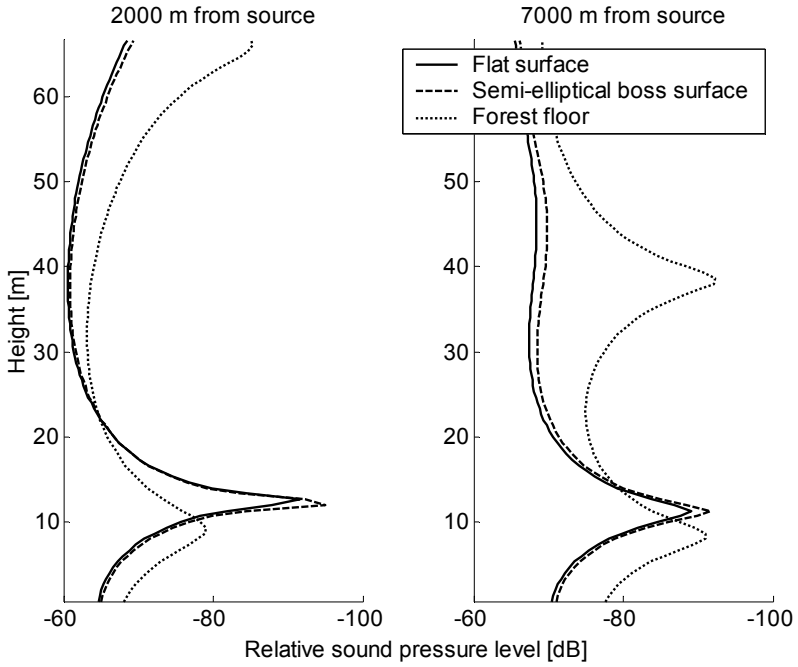

Figure 26 Relative sound pressure level at 2000 and 7000 m from the source for a flat, totally reflecting surface, the semi-elliptical boss surface (Z = 172.92070 + 108.74228i) and a forest floor (Z = 10.0800 +11.9000i). The sound speed profile is logarithmic with weak downward refraction (profile 1) in all cases. The graphs show how the sound pressure level is at a maximum at the surface.

One important feature of the boss surfaces and the natural ground surfaces used in these calculations is that the imaginary part of the impedance is positive. As said in chapter 4.2.1, positive reactance is one of the criteria for the existence of surface waves. While the reactance in theses cases is too high to develop a surface wave, the spring-like behaviour of a surface with positive reactance still causes a sound pressure level maximum at the ground level.

8.2. Varying sound speed profiles

The effects of refraction are examined by doing calculations with varying sound speed profiles, using the semi-elliptical boss surface to model the water surface. The sound speed profiles are described in chapter 7.3.

In figure 27 logarithmic sound speed profiles with varying refraction strengths are compared.

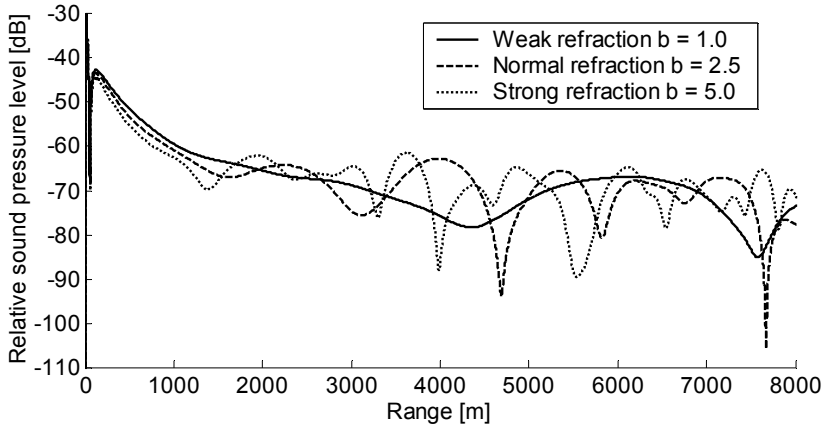

Figure 27 The relative sound pressure level calculated in downwind conditions using varying logarithmic sound speed profiles (profile 1, 2 and 3) and the semi-elliptical boss surface (Z = 172.92070 + 108.74228i). The receiver height is 1.33 m.

As can be seen in figure 27, stronger refraction leads to a more complex interference pattern. This is expected since increased refraction leads to smaller radius of the sound rays and more reflections for each ray. In figure 28, the logarithmic sound speed profiles 1 and 2 are compared with the low level jet profile (profile 4)

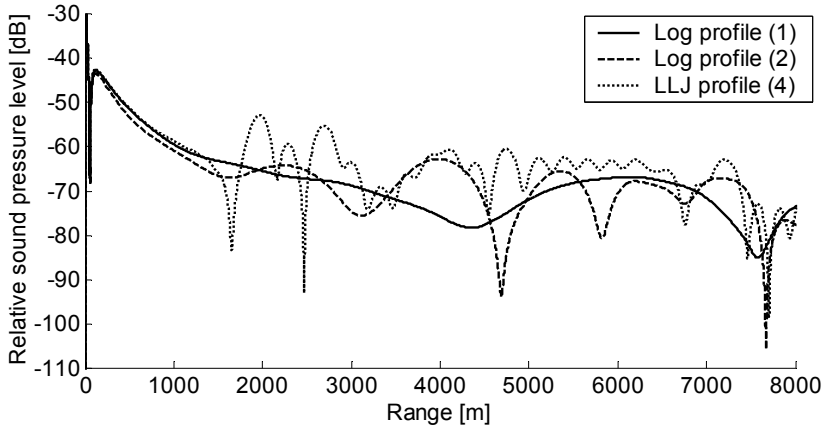

Figure 28 The relative sound pressure level calculated in downwind conditions using logarithmic sound speed profiles (1 and 2) and a sound speed profile with a low level jet (profile 4). The ground surface is the semi-elliptical boss surface (Z = 172.92070 + 108.74228i) and the receiver height is 1.33 m.

The low level jet gives rise to a strong interference pattern and the sound pressure level is at some points more than 10 dB higher than for the logarithmic profiles. Disregarding the most extreme values, the LLJ generally leads to sound pressure levels that are a couple of decibels higher than for the normal logarithmic profile (profile 2).

The interference is clearly visible in a colour plot. Figure 29 shows the propagation with the normal logarithmic sound speed profile (profile 2) and the semi-elliptical boss surface. It is easy to see how channelling occurs during these conditions.

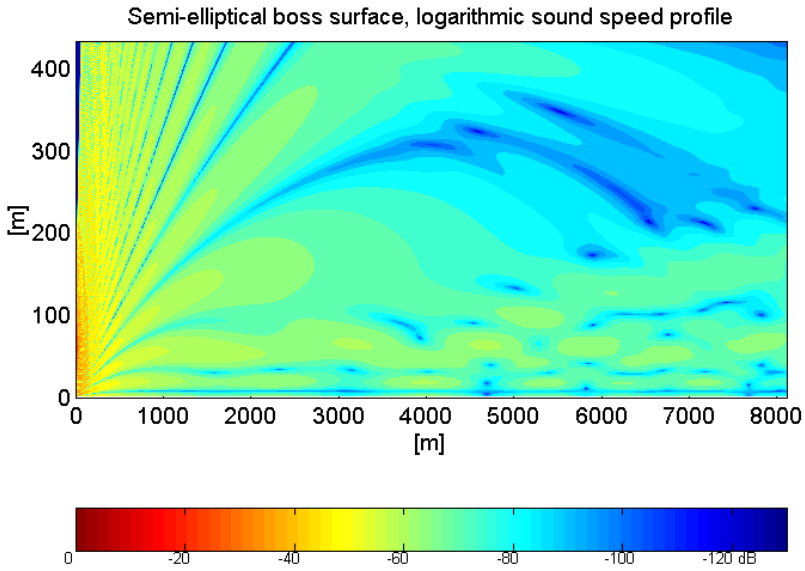

Figure 29 Calculation of the relative sound pressure level for a logarithmic sound speed profile with downwards refraction (profile 2) and the semi-elliptical boss surface (Z = 172.92070 + 108.74228i).

If a low level jet is present the channelling becomes even more obvious. The sound rays are effectively bended downwards by the layer at 200 m height where the sound speed is at its maximum (figure 30).

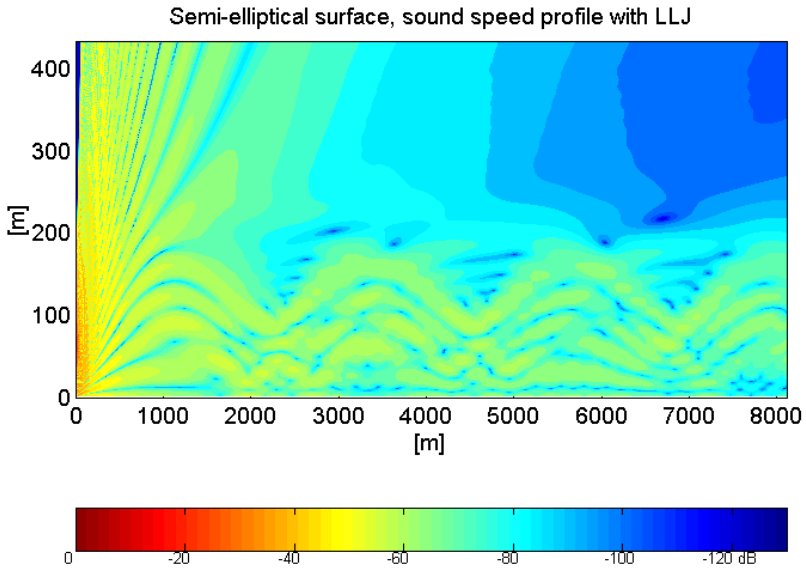

Figure 30 Calculation of the relative sound pressure level for a downwards refracting atmosphere with a low level jet (profile 4) and the semi-elliptical boss surface (Z = 172.92070 + 108.74228i).

8.3. Introducing a shore line

When a shore line is introduced, two major things happen; the sound speed is reduced due to greater friction from the ground surface and the ground boundary condition is changed. These two aspects shall first be considered separately.

In figure 31 a low level jet reaches a shore line at 4000 m range. The low level jet is assumed to slow down, first to the modified LLJ profile (profile 6) at 4000 m range, and then, at 4500 m range, to the logarithmic profile for inland conditions (profile 5).

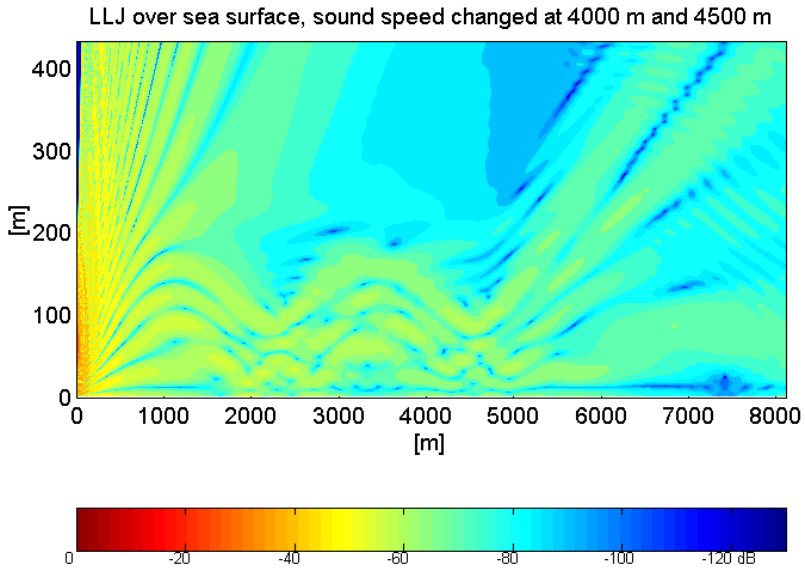

Figure 31 The relative sound pressure level calculated for a case where a LLJ reaches a shore line at 4000 m, the semi-elliptical boss surface is used for the whole calculation range (Z = 172.92070 + 108.74228i).

Figure 31 shows how the channelling is dissolved when the low level jet slows down. A similar pattern appears for the logarithmic sound speed profile 2 and 3 (normal and strong refraction). Figure 32 shows how the relative sound pressure level at 1.33 m height is reduced compared to a case with a constant low level jet throughout the whole calculation range.

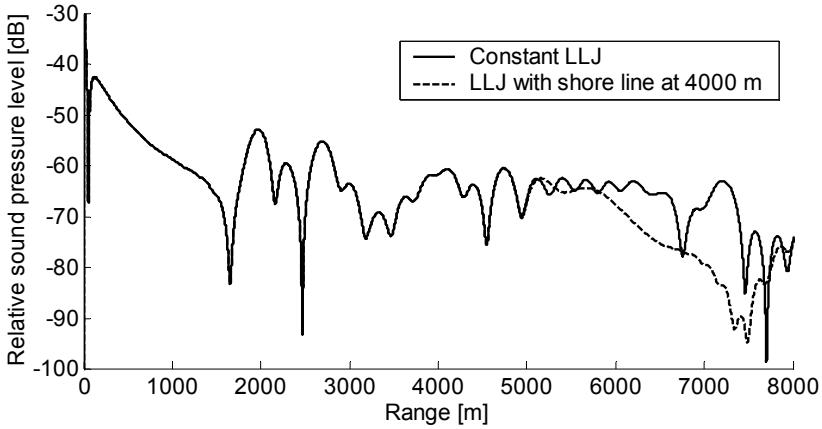

Figure 32 Calculation of relative sound pressure level for a case with a sound speed profile with a low level jet (profile 4) that reaches a shore line at 4000 m and slow down in two steps, (first to a modified LLJ (profile 6) and then, at 4500 m, to a logarithmic sound speed profile (profile 5)) compared with a case with a constant low level jet. The semi-elliptical boss surface is used for the whole calculation range (Z = 172.92070 + 108.74228i).

As can be seen in figure 32, the sound pressure level is decreased quite significantly after the sound speed profile is changed.

Changing the ground conditions, from a water surface covered with waves to a natural ground surface, also creates a reduction of the sound level. Figure 33 depicts the sound pressure level at 1.33 m height with normal downwards refraction. At 4000 m the ground is changed from the semi-elliptical boss surface to a forest floor. This is compared to the case with constant ground conditions.

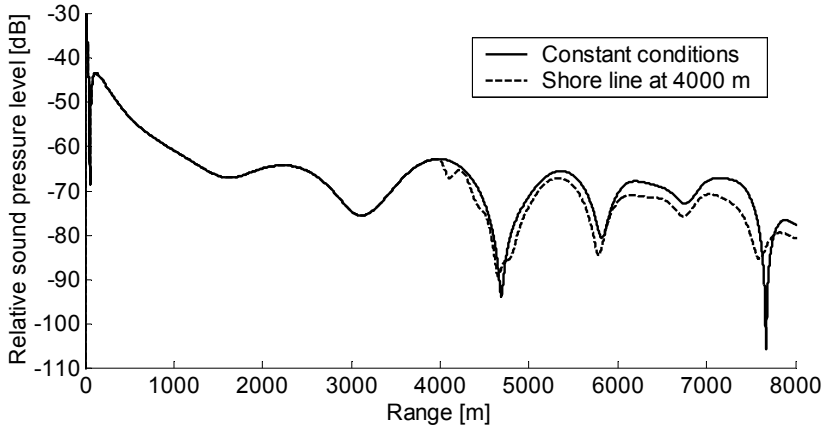

Figure 33 Calculation of relative sound pressure level for two cases with a logarithmic sound speed profile (profile 2). In one case the ground conditions change at 4000 m from the semi-elliptical boss surface (Z = 172.92070 + 108.74228i) to a forest floor (Z = 10.0800 +11.9000i), in the other case the ground conditions are kept constant (Z = 172.92070 + 108.74228i).

Figure 33 show how the change in impedance at 4000 m causes a reduction of the sound pressure level. There is a distinct minimum just after the shore line and then the sound pressure level stays a couple of decibel lower than for the constant case. This behaviour is even clearer when looking at the results from a calculation with the same ground conditions but with weak downwards refraction (profile 1).

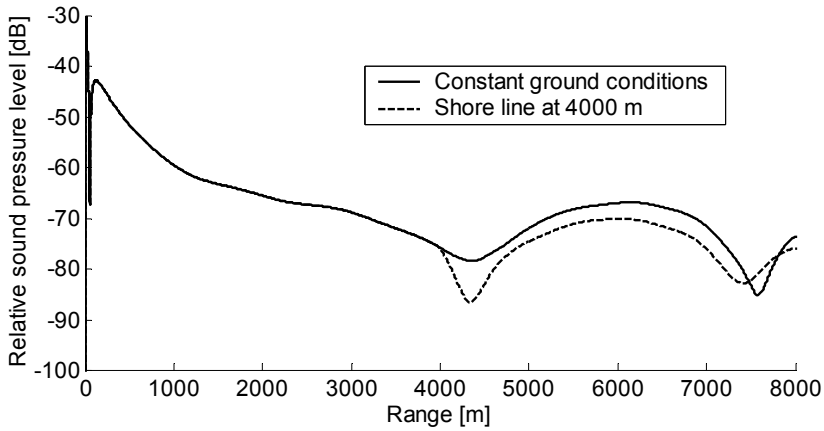

Figure 34 Calculation of relative sound pressure level for two cases with a logarithmic sound speed profile (profile 1). In one case the ground conditions change at 4000 m from the semi-elliptical boss surface (Z = 172.92070 + 108.74228i) to a forest floor (Z = 10.0800 +11.9000i), in the other case the ground conditions are kept constant (Z = 172.92070 + 108.74228i).

Figure 35 shows a colour plot of the sound pressure level in the whole calculation area for the case with normal refraction (profile 2) and a shore line at 4000 m.

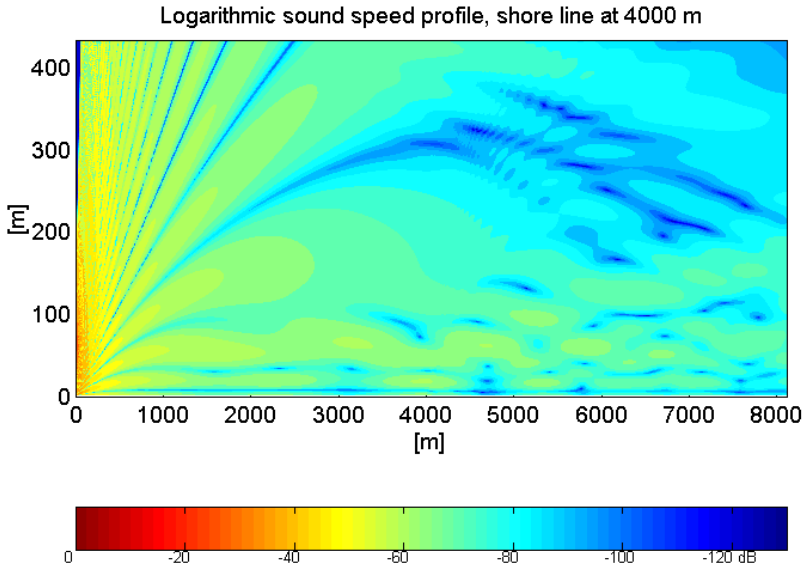

Figure 35 Relative sound pressure level calculated for a constant logarithmic sound speed profile (profile 2). The ground is changed from a semi-elliptical boss surface (Z = 172.92070 + 108.74228i) to a forest floor (Z = 10.0800 +11.9000i) at 4000 m.

The impedance discontinuity at 4000 m creates diffraction. This is expected but the diffraction pattern visible straight above the discontinuity is outside the angle restriction of the PE-model and might therefore be unrealistic. The sound field should nevertheless be accurate close to the ground.

In figure 30 both the sound speed and the ground is changed at the shore line. The sound speed over the sea is assumed to be logarithmic with normal refraction (profile 2) and the water surface is represented by the semi-elliptical boss surface. Over land the sound speed profile is changed slightly (profile 5) and the ground is changed to a forest floor.

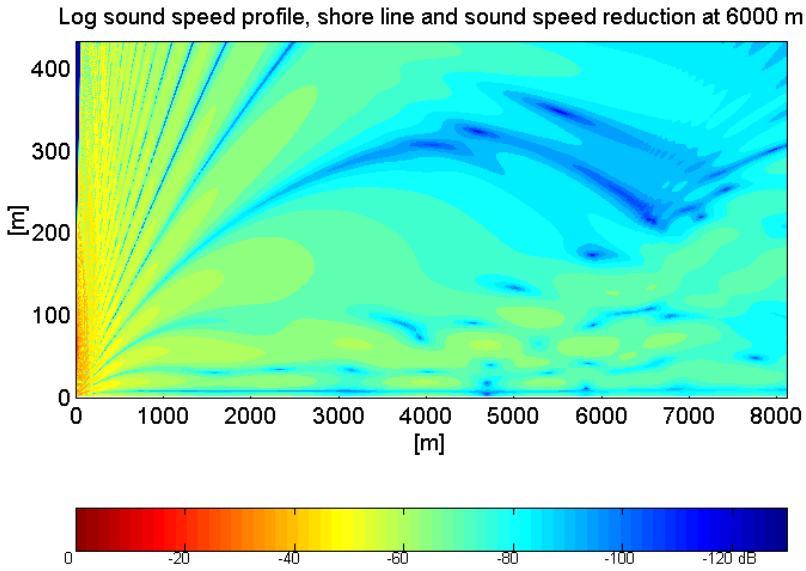

Figure 36 Relative sound pressure level calculated for a logarithmic sound speed profiles (profile 2 and, from 6000 m, profile 5). The ground is changed from the semi-elliptical boss surface (Z = 172.92070 + 108.74228i) to a forest floor (Z = 10.0800 +11.9000i) at 6000 m.

The sound pressure level at 1.33 m height for this case is shown in figure 37, compared to the case with a constant sound speed profile (profile 2) and constant ground conditions (semi-elliptical boss profile).

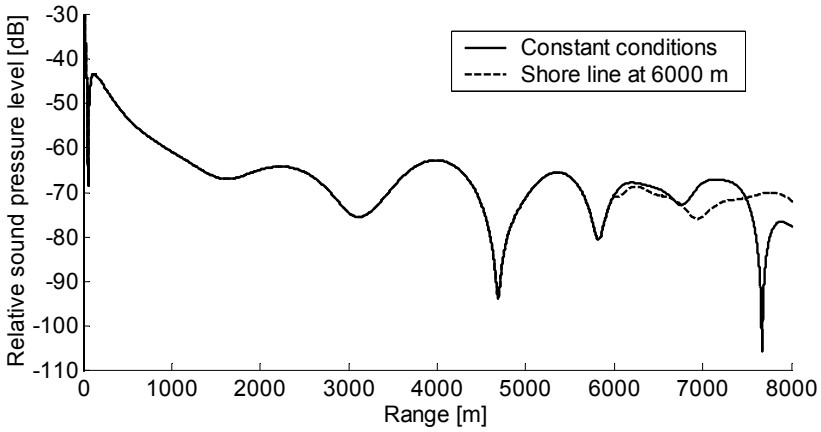

Figure 37 Relative sound pressure level for a case with a shore line at 6000 m where the sound speed profile is changed from profile 2 to profile 5 and the ground is changed from the semi-elliptical boss surface (Z = 172.92070 + 108.74228i) to a forest floor (Z = 10.0800 +11.9000i), compared with a case with constant conditions (profile 2 and semi-elliptical boss surface).

The same calculations are made for a case with a low level jet over the sea (figure 32). The sound speed profile is changed again in two steps, at 6000 m it is changed to the modified LLJ profile (profile 6) and at 6500 m it is changed to the logarithmic profile used for inland conditions (profile 5). The ground properties are changed at 6000 m from the semi-elliptical boss surface to a forest floor.

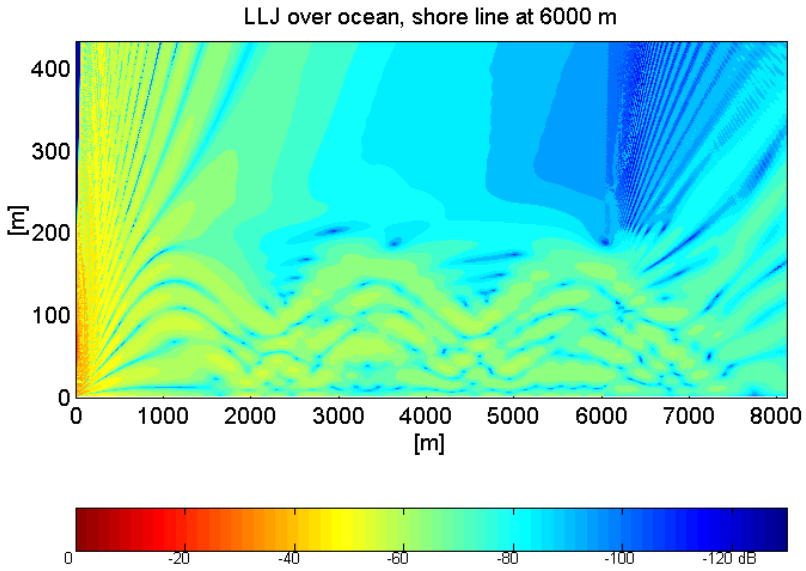

Figure 38 The relative sound pressure level is calculated for low level jet conditions over the sea. At the shore line the ground conditions are changed from the semi-elliptical boss surface (Z = 172.92070 + 108.74228i) to a forest floor (Z = 10.0800 +11.9000i).

The interference pattern is quite complex for this case due to both strong downwards refraction over the sea and the diffraction from the impedance discontinuity. Looking at 1.33 m height a sound level reduction is still apparent after introducing the shore line.

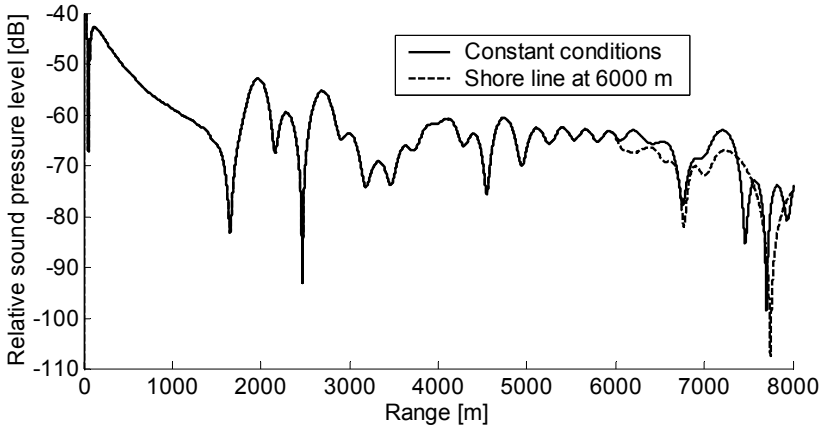

Figure 39 Relative sound pressure level for a case with a shore line at 6000 m where the sound speed profile is changed from profile 4 to profile 5 in two steps and the ground is changed from the semi-elliptical boss surface (Z = 172.92070 + 108.74228i) to a forest floor (Z = 10.0800 +11.9000i), compared with a case with constant conditions (profile 4 and the semi-elliptical boss surface).

8.4. Comparison with cylindrical propagation

In figure 40 the relative sound pressure levels using logarithmic and low level jet sound speed profiles are compared to the sound pressure level obtained assuming cylindrical propagation.

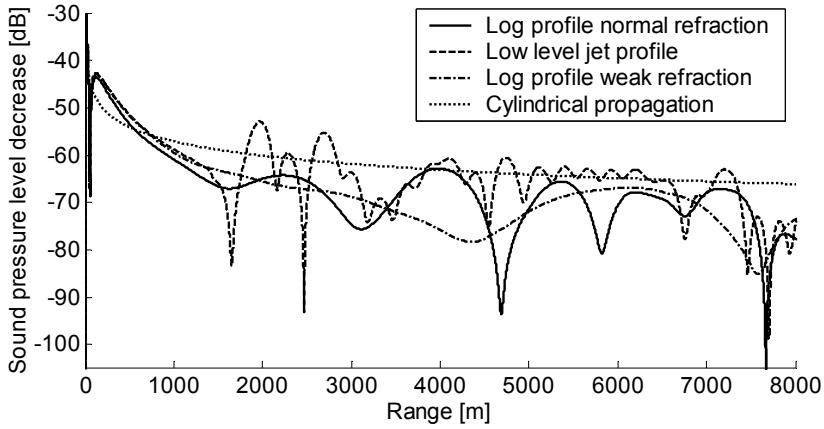

Figure 40 Calculations compared to cylindrical propagation.

The expression for the cylindrical propagation used here is:

$$L_p = L_w - 8 - 20 * \log x + 10 * \log \frac{x}{200} \qquad (76)$$

which gives spherical propagation up to 200 m from the source and then cylindrical propagation. [1] In figure 35 L_w is set to 7.5 dB according to chapter 8.

The desert measurements presented in Hubbard and Shepherd (1991) (see figure 2) also show cylindrical propagation at long ranges. In their case the spherical propagation seems to end at 300 m from the source. This would lead to sound pressure levels that are 10*log(300/200) = 1.8 dB lower than equation (76).

Disregarding the interference pattern, cylindrical propagation seems to be a very good approximation for both normal downward refraction and low level jet conditions at long ranges from the source.

[1] This kind of propagation model is suggested by The Swedish Environmental Protection Agency (report 6241) to be used when calculating noise from off-shore wind turbines.

9. Conclusions

In order to predict sound pressure levels from off-shore wind turbines, sound propagation mechanisms have been thoroughly investigated as well as relevant meteorology. An important aspect has been to investigate the effects of water waves on sound propagation; scattering by rough surfaces has therefore been studied as well as water wave theory.

A wide-angle CNPE model has been developed and validated against benchmark cases. To include water wave roughness, a boss model has been used which incorporates roughness in the impedance of the ground. Even though the boss model has a size restriction, the wave climate of the Baltic Sea is such that the boss model can be used frequently.

Calculations have been made for varying surface conditions and sound speed profiles. The effect of the water waves has been found to be small and the sea surface behaves more or less like a flat, hard surface. This means that the sound pressure level is at a maximum at the ground surface.

In downwind conditions there will be channelling of the sound which supports long-range sound propagation. Low level jets create especially strong downward refraction and the sound propagation in these cases will become cylindrical, which leads to a sound level decrease of only 3 dB per distance doubling. Logarithmic wind speed profiles with normal refraction strength also leads to cylindrical propagation even though the sound pressure levels will be somewhat lower than for low level jet conditions.

When the sound reaches a shore line the sound pressure level is generally decreased with a couple of decibels compared to continuing propagation over the sea. This is due both to changing ground conditions and generally lower wind speed.

The calculations agree well with existing measurements. These measurements are however somewhat incomplete and it is still unclear how common cylindrical propagation is. Long term measurements of sound from off-shore wind turbines including meteorological conditions would therefore be much helpful for the continuing work.

References

Attenborough K., Taherzadeh S.,Bass H. E., Di X., Raspet R., Becker G. R., Güdesen A., Chrestman A., Daigle G. A., L'Espérance A., Gabillet Y., Gilbert K. E., Li Y. L., White M. J., Naz P., Noble J. M., van Hoof H. A. J. M. (1995) Benchmark cases for outdoor sound propagation models, J. Acoust. Soc. Am. 97(1), pp 173-191

Attenborough K., Waters-Fuller T. (2000) Effective impedance of rough porous ground surfaces, J. Acoust. Soc. Am. 108(3), pp 949-956

Bergdahl L., Professor in Hydraulics at Chalmers University of Technology, Gothenburg, correspondence during 2002.

Biot M. A. (1968) Generalized boundary condition for multiple scatter in acoustic reflection, J. Acoust. Soc. Am. 44(6), pp 1616-1622

Boulanger P., Attenborough K., Taherzadeh S., Walters-Fuller T. (1998) Ground effect over hard rough surfaces, J. acoust. Soc. Am. 104(3), pp 1474-1482

Burke J. E., Twersky V. (1966) Scattering and reflection by elliptically striated surfaces, J. Acoust. Soc. Am. 40(4), pp 883-895

Chandler-Wilde S. N., Hothersall D. C. (1985) Sound propagation above and inhomogeneous impedance plane, J. Sound Vib. 98(4), pp 475-491

Daigle G. A., Piercy J. E., Embleton T. F. W. (1983) Line-of-sight propagation through atmospheric turbulence near the ground, J. Acoust. Soc. Am. 75(5), pp 1505-1513

Daigle G. A., Embelton T. F. W. (1990) Air-ground interface: surface waves, surface impedance and acoustic-to-seismic coupling coefficient, Proc. 4th Int. Symp. on Long-Range Sound Propagation, pp 27-40

Daigle G. A, Stinson M. R., Havelock D. I. (1996) Experiments on surface waves over a model impedance plane using acoustical pulses, J. Acoust. Soc. Am. 99(4), pp 1993-2005

Delany M. E., Bazley E. N. (1970) Acoustical properties of fibrous absorbent materials, Applied Acoustics 3, pp 105-116

Embelton T. F. W, Piercy J. E., Daglie G. A. (1983) Effective flow resistivity of ground surfaces determined by acoustical measurements, J. Acoust. Soc. Am. 74(4), pp 1239-1244

Embleton T. F. W. (1996) Tutorial on sound propagation outdoors, J. Acoust. Soc. Am. 100(1), pp 31-48

L'Espérence A., Herzog P., Daglie G. A., Nicolas J. R. (1992) Heuristic model for outdoor sound propagation based on an extension of the geometrical ray theory in the case of a linear sound speed profile, Applied Acoustics 37, pp 111-139

L'Espérance A., Gabillet Y., Daglie G. A. (1995) Outdoor sound propagation in the presence of atmospheric turbulence: Experiments and theoretical analysis with the fast field algorithm, J. Acoust. Soc. Am. 98(1) , pp 570-579

Hubbard H. H., Shepherd K. P. (1991) Aeroacoustics of large wind turbines, J. Acoust. Soc. Am. 89 (6), pp 2495-2508

Khandekar M. L. (1989) Operational analysis and prediction of ocean wind waves, Springer Verlag, New York

Kragh J., Plovsing B., Storeheier S. Å., Taraldsen G., Jonasson H. G. (2002) Nordic environmental noise prediction methods, Nord2000, Summary report, General Nordic sound propagation model and applications in source-related prediction methods, Delta Report AV 1719/01

Källstrand B. (1998) Low level jets in a marine boundary layer during spring, Conrt. Atmos. Phys. 71, pp 359-373

Lange B., Højstrup J. (1999) The influence of waves on the offshore wind resource, 1999 European Wind Energy Conference Proc., pp 1216-1219

Larsson C. (1997) Atmosfärisk absorption av ljud, svenska normalförhållanden (in Swedish), Meteorologiska Institutionen, Uppsala Universitet

Lee D., McDaniel S. T. (1987) Ocean acoustic propagation by finite-difference methods, Comput. Math. Applic. 14(5), pp 305-423

Li K. M. (1996) Propagation of sound above an impedance plane in a downward refracting atmosphere, J. Acoust. Soc. Am. 99, pp 746-754

Li K. M, Taherzadeh, S., Attenborough K. (1998) An improved ray-tracing algorithm for predicting sound propagation outdoors, J. Acoust. Soc. Am. 104(4), 2077-2083

Ljunggren S. (1999) Ljudutbredning kring havsbaserade vindkraftverk. Resultat från en litteraturstudie (in Swedish), Department of Civil and Architectural Engineering, KTH, Stockholm, AR 1999:6

Medwin H., D'Spain G. L., Childs E., Hollis S. J. (1984) Low-frequency grazing propagation over periodic steep-sloped rigid roughness elements, J. Acoust. Soc. Am. 76(6), pp 1774-1790

Mårtensson N, Bergdahl L. (1987) On the wave climate in the southern Baltic, Report Series A:15, Department of Hydraulics, Chalmers University of Technology, Gothenburg

Ogilvy J. A. (1991) *Theory of wave scattering from random rough surfaces*, Adam Hilger, Bristol

Ostashev V. E. (1997) *Acoustics in moving inhomogeneous media*, E&FN Spon, London

Pierce A. D. (1991) *Acoustics, An introduction to its physical principles and applications*, The Acoustical Society of America, New York

Raspet R., Sprague M. (1990) Exponential ground impedance models and their interpretations, Proc. 4th Int. Symp. on Long-Range Sound Propagation, pp 41-50

Raspet R., Wu W. (1995) Calculation of the average turbulence effects on sound propagation based on the fast field program formulation J. Acoust. Soc. Am. 97(1), 147-153

Raspet R., L'Espérance A. & Daigle G. A. (1995) The effect of realistic ground impedance on the accuracy of ray tracing, J. Acoust. Soc. Am. 97(1), pp 154-158

Reinius E. (1963) *Vattenbyggnad del 4 - Hamnar och farleder*, Acoprint Stockholm

Robertson J. S., Schlatter P. J., Siegmann W. L. (1996) Sound propagation over impedance discontinuities with the parabolic approximation, J. Acoust. Soc. Am. 99(2), pp 761-767

Sack R. A., West M. (1995) A parabolic equation for sound propagation in two dimensions over any smooth terrain profile: the generalised terrain parabolic equation (GT-PE), Applied Acoustics 45, pp 113-129

Salomons E. M. (1998) Caustic diffraction fields in a downward refracting atmosphere, J. Acoust. Soc. Am. 104(6), pp 3259-3272

Salomons E. M. (2001*) Computational atmospheric acoustics*, Kluwer Academic Publishers, Dordrecht

Schmidt H., Seong W., Goh J. T. (1995) Spectral super-element approach to range-dependent ocean acoustic modelling, J. Acoust. Soc. Am. 98, pp 465-472

Spera D. A. (1994) *Wind turbine technology*, ASME Press, New York

Stinson M. R., Daigle G. A. (1997) Surface wave formation at an impedance discontinuity, J. Acoust. Soc. Am. 102(6), pp 3296-3275

Taherzadeh S., Attenborough K., Li K. M. (2001) A hybrid BIE/FFP scheme for predicting barrier efficiency outdoors, J. Acoust. Soc. Am. 110(2), pp 918-924

Tolstoy I. (1984) Smoothed boundary condition, coherent low-frequency scatter, and boundary modes, J. Acoust. Soc. Am. 75(1), pp 1-22

West M., Gilbert K., Sack R. A. (1992) A tutorial on the parabolic equation (PE) model used for long range sound propagation in the atmosphere, Applied Acoustics 37, pp 31-49

Wilson D. K., Brasseur J. G., Gilbert K. E. (1999) Acoustic scattering and the spectrum of atmospheric turbulence, J. Acoust. Soc. Am. 105(1), pp 30-34

Wilson D. K (2000) A turbulence spectral model for sound propagation in the atmosphere that incorporates shear and buoyancy forcings, J. Acoust. Soc. Am. 108(5), pp 2021-2038

Appendix 1

Matlab code: CNPEWIDE.M

```
%-- Wide-angle PE - from Tutorial by M. West

clear;
%-- f - frequency
f = 50;

%-- dz – calculation step in z-direction
%-- dx – calculation step in x-direction
dz = 2/3;
dx = 2/3;

%-- nx – calculation range in x-direction
%-- nz – calculation range in z-direction
nx = 8110/dx;
nz = 650/dz;

%-- allocation of large matrises (saves computer time)

p = zeros(nz,nx+1);
pp = zeros(nz,nx);
Lp1 = zeros(nz,nx);

%-- zs - Source height (in meters)
zs = 65;
nzs = round(zs/dz);

%-- (logarithmic) sound speed gradient
```

```
b = 1;
z0 = 0.5;
c = 340 + b*log(1+dz*[0:nz-1]/z0);

%-- wave number
k0 = 2*pi*f/340;
km = 2*pi*f./c;

%-- surface impedance
Zg = 172.92070 + 108.74228i

%-- ground boundary condition
if isinf(Zg) == 1
   s1 = 4/3;
   s2 = -1/3;
else
   s1 = 4/(3-2*i*k0*dz/Zg);
   s2 = -1/(3-2*i*k0*dz/Zg);
end

%-- attenuation in the upper region
natt = round(50*340/f);
At = 0.242;

for n = nz-natt:nz
   km(n) = km(n) + i*At*((n-nz+natt)^2/natt^2);
end

%-- Upper boundary condition
Zu = 1;
su1 = 4/(3 - 2*i*k0*dz/Zu);
su2 = -1/(3 - 2*i*k0*dz/Zu);
```

```
%-- creation of matrises

e=ones(nz,1);
B=[e -2*e e];
T=spdiags(B, -1:1,nz,nz);
T(1,1)=T(1,1)+s1;
T(1,2)=T(1,2)+s2;
T(nz,nz)=T(nz,nz)+su1;

I=spdiags(e,0,nz,nz);

a=i/(2*k0*dz^2);
b=i*(km.^2-k0^2)/(2*k0);

D=spdiags(conj(b'),0,nz,nz);

M1=I+dx/2*(a*T+D)+(a*T+D)/(2*i*k0);
M2=I-dx/2*(a*T+D)+(a*T+D)/(2*i*k0);

M=full(inv(M2)*M1);

%-- Generation of point source
A0 = 1.3717;
A2 = -0.3701;
B = 3;

if isinf(Zg) == 1
   C = 1;
else
   C = (Zg-1)/(Zg+1);
end

for n=1:nz
```

```
p(n,1)=sqrt(i*k0)*(A0+A2*k0^2*(n*dz-zs)^2)*exp(-k0^2*(n*dz-zs)^2/B)+
C*sqrt(i*k0)*(A0+A2*k0^2*(n*dz+zs)^2)*exp(-k0^2*(n*dz+zs)^2/B);
end

%-- Calculation of sound pressure
for n = 2:nx+1
   xx = (n-1)*dx;
   p(:,n) = M*p(:,n-1);
   pp(:,n-1) = p(:,n)/sqrt(xx);
end

clear p M M1 M2

%-- Calculation of sound pressure level relative to source strength and
%-- limitation of sound level to -120 dB

psinv = 1/abs(pp(nzs,1));

for m = 1:nz
   for n = 1:nx
      if abs(pp(m,n))<=1e-6
         pp(m,n)=1e-6;
      end
      Lp1(m,n)=20*log10(psinv*abs(pp(m,n)));
   end
end

%-- saving data
save('D:\matlab\data\test.dat','Lp1','-ASCII');
```